Acute IFN-γ responses drive sensory neuron injury and chronic pain after chikungunya virus infection

Lilian C. Colodeti[1,2], Thamires B. P. Gonçalves[2], Hannah P. Mota-Araujo[1], Suzana M. B. Araujo[1,2], Greice N. Pires[3], Bruno V. M. Santiago[4], Thiago S. Bacelar[1,2], Fabricia L. Fontes-Dantas[5], Emily C.C. Rennô[1,2], Mariana O. L. da Silva[6], Luiz Eduardo B. Savio[1], Pedro S. Ciriaco[3], Tiago B. Taboada[3], Ana B. O. Barbosa[1], Fabio M. Gomes[1], Ana M. B. Martinez[3], Iranaia M. Assunção[6], Nivaldo R. Villela[4], José Proença-Modena[8], William M. de Souza[9], Henrique R. Mendonça[7], Soniza Alves-Leon[1, 3, 10], Giselle F. Passos[2], Robson da Costa[2]*, Claudia P. Figueiredo[1,2]*

1 Carlos Chagas Filho Institute of Biophysics, Federal University of Rio de Janeiro, Rio de Janeiro, Brazil.
2 School of Pharmacy, Federal University of Rio de Janeiro, Brazil.
3 Clementino Fraga Filho University Hospital, Federal University of Rio de Janeiro, Rio de Janeiro, Brazil.
4 Center of Pain, Rio de Janeiro State University, Rio de Janeiro, RJ, Brazil.
5 Department of Pharmacology and Psychobiology, Roberto Alcântara Gomes Institute Biology, Rio de Janeiro State University, Brazil.
6 Institute of Microbiology Paulo de Goes, Federal University of Rio de Janeiro, Rio de Janeiro, Brazil.
7 Institute of Biodiversity and Sustainability NUPEM, Federal University of Rio de Janeiro, Macaé, Brazil.
8 Laboratory of Emerging Viruses, Department of Genetics, Microbiology and Immunology, Institute of Biology, University of Campinas, Campinas, São Paulo, Brazil.
9 Department of Microbiology, Immunology and Molecular Genetics, University of Kentucky, College of Medicine, Lexington, KY, USA.
10 Translational Neuroscience Laboratory (LabNet), Biomedical Institute, Federal University of the State of Rio de Janeiro, Brazil.

Abstract:
Chikungunya virus (CHIKV) infection frequently leads to persistent and debilitating pain, yet the mechanisms linking early antiviral responses to long-term sensory dysfunction remain unclear. Here, we identify interferon-γ (IFN-γ) as a key determinant of chronic pain after CHIKV infection. Using an intra-articular infection model, we show that CHIKV induces sustained joint inflammation, cartilage catabolism, and sensory neuron injury signatures, including *Atf3* upregulation, in the absence detectable viral dissemination to dorsal root ganglia (DRG). IFN-γ expression was markedly elevated in infected joints, and direct IFN-γ administration was sufficient to induce mechanical hypersensitivity and neuronal stress independently of joint degeneration. Conversely, genetic or pharmacological disruption of IFN-γ signalling prevented CHIKV-induced pain and neuronal stress without altering viral burden, demonstrating that IFN-γ is required for both sensory dysfunction and joint pathology. To model clinical heterogeneity, we stratified infected mice based on long-term nociceptive profiles and identified a persistent-pain subgroup characterized by elevated acute-phase systemic IFN-γ and chronic peripheral neuropathic features. In a prospective patient cohort. In a prospective patient cohort, acute-phase IFN-γ levels discriminated individuals who later developed chronic arthralgia from those who recovered, whereas IL-6, IL-1β, and TNF-α were unchanged, mirroring the signature observed in mice. Together, these findings define an IFN-γ–driven neuroimmune mechanism underlying persistent pain after CHIKV infection and identify IFN-γ as a biomarker and a promising therapeutic target.

Keywords: Sensory neuron injury; dorsal root ganglia; neuropathic pain; viral arthritis; chronic arthralgia, alphavirus.

Introduction

Chikungunya virus (CHIKV) is a mosquito-transmitted, arthritogenic alphavirus that has caused over 35 million suspected or confirmed infections across more than 100 countries [1-3], now representing a global health concern due to climate-driven expansion of Aedes vectors beyond the Global South[4]. CHIKV infection typically presents with a self-limited acute febrile illness with nonspecific viral symptoms, followed in a substantial proportion of individuals by persistent articular manifestations. While subacute symptoms may last several weeks, chronic disease is marked by often debilitating polyarthralgia and polyarthritis that can persist for months or years[3,5-8], imposing a significant long-term socioeconomic burden on affected individuals and health systems. Furthermore, CHIKV infection can also result in neurological manifestations ranging from neuropathic pain to encephalitis[9-13], as well as severe and occasionally fatal outcomes[14]. At present, Ixchiq (formerly VLA1553) and Vimkunya (formerly PXVX0317) are the two licensed vaccines in the United States, European Union, and Brazil[15]; however, the use of Ixchiq was recently suspended in the USA due to severe adverse effects in elderly individuals[16,17].

Beyond the acute febrile illness, CHIKV infection is frequently complicated by chronic, often debilitating arthralgia that can persist for months or years, imposing a substantial long-term socioeconomic burden on affected individuals and health systems[3,5-8]. CHIKV infection can cause distinct acute, subacute, and chronic phases. The acute phase is characterized by fever, myalgia, headache, rash, and arthralgia lasting up to 3 weeks. Subacute disease involves persistent fatigue and articular symptoms lasting between 3 and 12 weeks, while chronic arthralgia is often debilitating polyarthralgia and polyarthritis that can persist for months or years[3,5-8]. Furthermore, CHIKV infection can also result in neurological manifestations ranging from neuropathic pain to encephalitis[9-13], as well as severe and occasionally fatal outcomes[14]. At present, Ixchiq (formerly VLA1553) and Vimkunya (formerly PXVX0317) are the two licensed vaccines in the United States, European Union, and Brazil[15]; however, the use of Ixchiq was recently suspended in the USA due to severe adverse effects in elderly individuals[16,17].

Previous studies have shown that IFN-γ levels increase during the acute phase of CHIKV infection[3,18-23]. However, whether these early IFN-γ responses influence the development of persistent joint pain remains unknown, as both clinical and experimental evidence linking acute inflammation to long-term pain outcomes is limited. In parallel, beyond its antiviral and immunomodulatory roles[24], IFN-γ has also been implicated in modulating nociceptive pathways, with studies showing that elevated IFN-γ signalling can enhance pain sensitivity and that its blockade mitigates pain behaviours[25,26]. Importantly, although CHIKV infection is increasingly associated with neuropathic features in patients[9,27-31], whether IFN-γ directly drives peripheral sensory neuron injury or instead contributes to the development of chronic neuropathic pain remains unclear. Consequently, the mechanisms linking acute joint inflammation, antiviral immunity, and the emergence of persistent pain remain poorly defined.

Here, we investigated whether IFN-γ acts as a mechanistic driver of chronic pain after CHIKV infection. Using an integrated clinical-experimental framework, we demonstrate that elevated acute-phase IFN-γ levels are associated with persistent arthralgia in patients and are sufficient to induce neuronal stress and mechanical hypersensitivity in mice. Conversely, genetic or pharmacological disruption of IFN-γ signalling attenuated CHIKV-induced pain, establishing IFN-γ as a critical mediator linking antiviral inflammation to long-term nociceptive outcomes. Together, these findings identify IFN-γ as a key determinant of chronic pain trajectories following CHIKV infection and reveal a mechanistic axis connecting acute immune responses to persistent sensory dysfunction.

Results

CHIKV infection triggers joint pathology and sensory neuron stress

To dissect the pathophysiology of CHIKV-induced pain under immunocompetent conditions, we develop an intra-articular (i.a.) inoculation model (Figure 1A), in which 10^6 PFU of CHIKV (strain BHI3768) were injected into the knee joint. This approach mimics the natural tropism of the virus for articular tissues in humans. We first confirmed local viral replication and distribution. CHIKV RNA was detected in both ipsilateral and contralateral knees, with significantly higher levels in the ipsilateral knee. Viral RNA peaked at 1-day post-infection (dpi) and remained elevated for at least 28 dpi (Figure 1B). Infectious viral particles were also recovered from ipsilateral knee tissue between 4h and 3 dpi, peaking at 1 dpi (Figure 1C), confirming productive replication. Immunolabeling of double-stranded RNA (dsRNA) further revealed strong viral signals (Figure 1D-E) within articular cartilage (Figure 1F) and synovial tissue (Figure 1G) at 28 dpi, while mock controls showed no signal (Figure 1D), demonstrating the persistence of viral RNA in joint compartments (Figure 1B, E-G).

We next evaluated the functional consequences of CHIKV infection. Infected mice exhibited significantly reduced ipsilateral paw withdrawal thresholds starting at 10 dpi and persisting through 28 dpi compared with mock controls (Figure 1H), and area-under-the-curve (AUC) analysis confirmed the persistence of mechanical allodynia (Figure 1I). In contrast, cold sensitivity did not significantly differ between CHIKV-infected and control mice across the same period (Figure 1J-K). To assess whether sex influenced pain development, we further analysed the same datasets separately for males and females (Figure S1). Both sexes exhibited a significant reduction in paw withdrawal thresholds following CHIKV infection compared with their respective controls (Figure S1A–D), indicating that mechanical allodynia develops robustly in both males and females. Cold sensitivity did not differ significantly at any individual time point in either sex (Figure S1E-H). Given the robust mechanical hypersensitivity and the absence of major sex-specific differences, mirroring the predominant joint pain observed in CHIKV patients, subsequent experiments were performed using mixed-sex cohorts.

Given that joint inflammation and tissue remodelling, including cartilage damage, are hallmarks of arthritis[32], we next examined whether CHIKV infection drives histopathological alterations in the knee. Histopathological analysis of knee sections revealed marked synovial hyperplasia, dense inflammatory infiltrates, and tissue disorganization compared with Mock controls (Figure S2A-B), accompanied by significantly higher histopathological scores at 7 and 28 dpi (Figure S2C-D). We also found a marked loss of proteoglycans in infected joints, as indicated by reduced safranin-O (Figure 1L-N) and toluidine blue staining (Figure 1O and Figure S2E-F) at 28 dpi. Consistent with these changes, CHIKV-infected knees showed elevated expression of *Mmp13* (a collagenase that degrades type II collagen; Figure 1P), and *Adamts4* (an aggrecanase that cleaves proteoglycans; Figure 1Q), two key enzymes implicated in cartilage destruction[33-35]. The *Rankl*/*Opg* mRNA ratio, an indicator of osteoclast activation and bone resorption [36], was also significantly elevated at 28 dpi (Figure 1R). Collectively, these findings show that CHIKV infection drives joint inflammation and elicits molecular signatures of cartilage and bone catabolism together with pain hypersensitivity, closely mirroring key aspects of human disease.

Clinical reports have documented neuropathic pain symptoms in patients infected with CHIKV[9-11,28-30], suggesting that mechanisms beyond inflammatory joint damage contribute to disease-associated pain. To probe this possibility, we tested whether CHIKV-induced mechanical allodynia was sensitive to gabapentin (GBP), a widely used treatment for neuropathic pain[37]. GBP robustly attenuated mechanical allodynia over time (Figure S2G) and reduced overall hypersensitivity (AUC analysis; Figure S2H), supporting a neuropathic component of CHIKV-evoked pain. We therefore next tested whether the pain phenotype involved sensory neuron injury. Expression of activating transcription factor 3 (*Atf3*), a canonical marker of neuronal stress and damage[38-41], was significantly upregulated in lumbar dorsal root ganglia (DRG) at both 7 and 28 dpi (Figure 1S), indicating sustained neuronal stress. To rule out direct viral

infection as a contributing factor, CHIKV RNA was quantified in lumbar DRGs but was largely undetectable at all-time points (Figure 1T). Collectively, these results indicate that CHIKV infection induces indirect sensory neuron injury and supports a neuropathic contribution to the persistent pain state.

IFN-γ and T cells drive joint inflammation in CHIKV-induced arthritis

We next characterized the inflammatory response in the CHIKV arthritis model, focusing on pro-inflammatory mediators and on the immune cells response for their production. qPCR analysis showed transient induction of *tnf-α* (Figure 2A) and *il-6* (Figure 2B) mRNA, peaking at 7 and 3 dpi, respectively. Type I interferons were likewise induced early, with *ifn-α* (Figure 2C) and *ifn-β* (Figure 2D) expression peaking at 1 dpi before returning to baseline. Notably, *ifn-γ* expression was strongly and persistently elevated, peaking at 7 dpi and remaining above Mock levels through at least 28 dpi (Figure 2E). These findings prompted us to identify the predominant immune cell populations in the joint and determine the main cellular source of IFN-γ.

To define the immune cell populations driving joint inflammation, we profiled synovial fluid and peripheral blood by flow cytometry. Joint fluid analysis revealed a pronounced influx of $CD4^+$ (Figure 2F-G) and $CD8^+$ T cells (Figure 2F-H) at 7 dpi, which largely resolved by 28 dpi. Myeloid cells ($CD11b^+CD45^+$) displayed a similar kinetic profile, peaking in the joint at 7 dpi and returning towards baseline by 28 dpi (Figure 2I–J). Concomitantly, circulating $CD11b^+CD45^+$ cells were significantly reduced at 7 dpi, consistent with recruitment from blood into the joint (Figure 2K). We next sought to identify the lymphocyte populations responsible for IFN-γ production within the joint. IFN-γ expression by NK cells was negligible (<2% IFN-$γ^+$ cells) at all-time points analysed (Figure S3A-B), whereas IFN-$γ^+$ $CD8^+$ T cells were markedly increased at 7 dpi (Figure 2L-M). IFN-$γ^+$ $CD4^+$ T cells also increased at 7 dpi, albeit to a lesser extent (Figure 2N-O). These data establish $CD8^+$ T cells as the predominant IFN-γ-producing lymphocyte population in the joint at the peak of inflammation.

IFN-γ drives neuronal stress and pain in CHIKV infection independent of joint degeneration

The marked and sustained induction of IFN-γ in the infected joint (Figure 2) highlighted this cytokine as a candidate mediator of CHIKV-evoked pain. To directly assess whether IFN-γ is sufficient to trigger joint pain hypersensitivity, we administered intra-articular (i.a.) recombinant IFN-γ to naïve mice. Repeated dosing (300 or 600 U/site, every two days for 7 days) induced a rapid and sustained mechanical allodynia in the von Frey test (Figure 3A–B). Given that both doses elicited similar behavioural responses, the lower dose (300 U/site) was chosen for subsequent molecular analyses. Despite this robust pain phenotype, the expression of *adamts4* (Figure 3C) and *mmp13* (Figure 3D) remained unchanged relative to vehicle-treated controls, indicating that IFN-γ is sufficient to elicit pain independently of structural joint tissue remodelling. The uncoupling of mechanical allodynia (Figure 3A-B) from joint degeneration (Figure 3C-D) supported to a neuronal basis for IFN-γ–evoked pain. Consistently, intra-articular IFN-γ significantly increased *Atf3* expression in lumbar DRGs (Figure 3E), supporting a direct capacity of IFN-γ to induce sensory neuron stress and pain-like behaviour without joint degeneration.

Given these *in vivo* findings, we next asked whether IFN-γ can directly act on sensory neurons to elicit activation and stress signalling. To address this, primary mouse DRG neurons were cultured and exposed to IFN-γ, and ERK phosphorylation (p-ERK) was assessed as a readout of neuronal activation [42,43], alongside ATF3 induction as an indicator of neuronal stress (Figure 3F–K). IFN-γ treatment led to a significant increase in p-ERK^+ neurons, as shown by co-immunostaining with NeuN (Figure 3F-G). Capsaicin, used as positive control, produced a similar rise in p-ERK levels, confirming neuronal responsiveness under our experimental conditions (Figure 3H). IFN-γ exposure also increased the proportion of $ATF3^+$ neurons, as demonstrated by double immunostaining with NeuN (Figure 3I-J), and qPCR analysis confirmed a robust upregulation of *Atf3* mRNA (Figure 3K). Together, these results indicate that IFN-γ directly activates DRG neurons and induces a transcriptional stress response.

Based on our findings that CHIKV infection induces robust IFN-γ responses (Figure 2) and that intra-articular IFN-γ is sufficient to elicit pain (Figure 3A-B), we next tested whether blocking IFN-γ signalling could attenuate pain development after CHIKV infection. To this end, we employed both pharmacological and genetic strategies to disrupt its signalling and examined the impact on nociceptive behaviour and DRG stress responses.

Dose-ranging experiments revealed that local administration of an anti-CD119 (IFN-γ receptor 1) monoclonal antibody produced comparable attenuation of mechanical allodynia across the tested doses (Figure S3C) and the higher dose was therefore selected for subsequent analyses. Intra-articular administration of the anti-CD119 monoclonal antibody significantly attenuated CHIKV-induced mechanical allodynia compared with isotype control (Figure 3L-M), while viral RNA levels in the joint remained unchanged at 21 dpi (Figure 3N), indicating that pain attenuation occurred independently of viral clearance. Anti-CD119 treatment also blunted CHIKV-induced upregulation of the catabolic genes *Adamts4* (Figure 3O) and *Mmp13* (Figure 3P), indicating suppression of joint catabolic remodelling programs. Consistently, *Ifng*$^{-/-}$ mice were similarly protected, maintaining baseline withdrawal thresholds through 21 dpi (Figure 3Q-R), with no change in joint viral RNA (Figure S3D). Notably, *ifn-γ* deficiency abolished the induction of a*damts4* (Figure 3S) and *mmp13* (Figure 3T) in the joint and *atf3* in the DRG (Figure 3U), indicating that IFN-γ signalling is required for both joint catabolic responses and neuronal stress associated with CHIKV infection. Together, these findings identify IFN-γ signalling as a key contributor to the development of CHIKV-induced pain.

Acute systemic IFN-γ responses predict persistent pain after CHIKV infection

Although recovery from CHIKV-induced arthralgia is typically rapid, a subset of patients develops prolonged pain, revealing striking variability in disease outcomes [44-47]. To determine whether this clinical divergence is mirrored in our intra-articular CHIKV infection model (Figure 4A) and to probe the contribution of IFN-γ to pain chronicity, we extended our analyses to later post-infection stages. Mechanical sensitivity assessed by the von Frey test revealed that mice receiving i.a. CHIKV injection (10^6 PFU) into the knee displayed markedly reduced ipsilateral paw withdrawal thresholds from 7 to 77 dpi compared with mock-infected controls, with significant differences observed between 14 and 42 dpi (Figure 4B). AUC analysis confirmed robust and sustained mechanical hypersensitivity in infected mice (Figure 4C). To model the heterogeneity observed in patients, we next stratified CHIKV-infected mice based on their mechanical sensitivity profiles. Animals with a ≥30% reduction from baseline (i.e., withdrawal thresholds ≤70% of baseline) were categorized as the persistent group (Persis., orange symbols), whereas those with a <30% reduction (>70% of baseline) were classified as the recovered group (Recov., blue symbols) (Figure 4D). This stratification allowed us to investigate the mechanisms underlying distinct pain outcomes. The persistent group (~50% of animals) maintained significantly lower withdrawal thresholds up to 77 dpi, indicating long-term pain, whereas recovered animals returned to baseline sensitivity by 49 dpi (Figure 4E). AUC analysis restricted to the chronic phase (42–77 dpi) showed that the persistent group exhibited a significantly reduced withdrawal threshold compared with both mock and recovered animals, whereas no difference was observed between mock and recovered groups (Figure 4F).

To assess whether persistent pain was linked to ongoing viral replication within peripheral tissues, we quantified CHIKV RNA in ipsilateral knee joints and lumbar DRGs at 77 dpi. CHIKV RNA levels were comparable between mice with persistent and recovered phenotypes (Figure 4G-H), suggesting that sustained viral replication is unlikely to underlie the maintenance of chronic pain. Similarly, expression of cartilage- and bone-catabolic genes *Mmp13* (Figure 4I), *Adamts4* (Figure 4J), and the *Rankl*/*Opg* mRNA ratio (Figure 4K) was comparable across groups, suggesting that structural joint degeneration is not associated with the maintenance of chronic pain. Together, these findings demonstrate that persistent pain following CHIKV infection occurs independently of viral persistence or ongoing structural joint degeneration.

Given the central role of IFN-γ in shaping antiviral immunity and modulating pain pathways, we next asked whether differential IFN-γ responses might underlie the distinct pain outcomes observed in CHIKV-infected mice. Notably, serum IFN-γ concentrations were significantly elevated in the persistent group during the acute phase compared with both recovered and Mock groups (Figure 4L). During the chronic phase, IFN-γ levels remained elevated but did not differ significantly between groups (Figure 4M). These findings indicate that increased systemic IFN-γ responses during the acute phase of CHIKV infection are associated with long-term pain in mice.

Persistent CHIKV pain associates with chronic peripheral neuropathic alterations

We next asked whether persistent pain after CHIKV infection, which is associated with increased IFN-γ responses, is accompanied by molecular and morphological changes in peripheral sensory structures when comparing recovered and chronically affected animals. *Atf3* mRNA levels in the DRG did not differ among persistent, recovered, and Mock groups at 77 dpi (Figure S4A), consistent with a transient *Atf*3 response that is not detectable at late stages when pain phenotypes are established. Cleaved caspase-3 activation in the DRG has been reported in experimental models of chronic pain[48-50]. We therefore examined cleaved caspase-3 in the DRG of persistent, recovered, and Mock animals after CHIKV infection and found a robust increase in cleaved caspase-3 immunoreactivity selectively in DRG neurons from animals with persistent pain (Figure 5A-B). We then asked whether DRG caspase-3 activation might translate into chronic morphological alterations in the sciatic nerve innervating the affected joint in animals with persistent pain. Quantification of myelinated fiber density in semi-thin sciatic nerve cross-sections revealed no significant differences among groups (Figure 5C and Figure S4B). Analysis of myelin morphology showed discrete alterations, such as vacuolizations (Figure 5D and Figure S4C) and myelin splitting (Figure 5D-E). Consistently, g-ratio distribution analysis revealed a significant reduction of fibres within the optimal 0.56–0.65 range in the CHIKV-persistent group compared with both recovered and mock controls (Figure 5F). Neurofilament 200 (NF200), a marker of large myelinated sensory axons[51], was assessed to determine whether persistent pain after CHIKV infection is associated with alterations in axonal integrity in the peripheral nerve. Immunofluorescence analysis of the sciatic nerve revealed a trend toward reduced NF200 signal intensity in animals with persistent pain compared with recovered animals, although this difference did not reach statistical significance (Figure S4D-E). Ultrastructural analysis by transmission electron microscopy further revealed marked myelin abnormalities in sciatic nerves from animals with persistent pain (Figure 5G). Whereas myelinated fibres from Mock and recovered animals displayed compact, concentrically arranged myelin lamellae with uniform periodicity and preserved axonal morphology, fibres from the persistent group showed pronounced myelin pathology, including extensive lamellar separation and decompaction, intramyelinic vacuolization, accumulation of electron-dense fibrillar material within split lamellae, and irregular myelin profiles with focal myelin unravelling (Figure 5G). Collectively, our findings demonstrate that persistent pain following CHIKV infection is accompanied by sustained caspase-3 activation in sensory neurons and by structural abnormalities of the myelin in the sciatic nerve, revealing a chronic peripheral neuropathic phenotype in the absence of gross fiber loss.

Elevated IFN-γ levels during acute CHIKV infection are associated with chronic pain outcomes in patients

To assess the translational relevance of our findings, we examined whether systemic cytokine responses during acute CHIKV infection are associated with persistent pain outcomes in patients. Serum levels of TNF, IL-6, IL-1β, and IFN-γ were measured in a prospective cohort of individuals who either recovered (CHIKV-recovery, n = 20) or developed chronic arthralgia (CHIKV-chronic, n = 22) three months after CHIKV infection (Figure 6A). We first evaluated whether acute-phase clinical symptoms were associated with the subsequent development of chronic arthralgia. Odds ratio analysis revealed that none of the acute-phase clinical symptoms showed a significant association with chronic outcome (Figure 6B).

Concentrations of TNF-α, IL-6, and IL-1β did not differ significantly between groups (Figure 6C, E e G), indicating that these classical inflammatory mediators are not associated with long-term pain outcomes. In contrast to other cytokines, IFN-γ levels measured during the acute phase were significantly higher in patients who subsequently developed chronic pain compared with those who recovered (Figure 6I). Receiver operating characteristic (ROC) analysis further demonstrated that IFN-γ displayed superior discriminative performance for chronic arthralgia compared with TNF-α, IL-6, and IL-1β (Figure 6D, F, H, J). Together, these results indicate that elevated IFN-γ during acute CHIKV infection is a shared feature of both experimental and clinical disease and is associated with an increased risk of persistent pain. By integrating mechanistic insights from animal models with clinical association and discriminative analyses, our findings support a role for IFN-γ–driven inflammatory responses in shaping long-term pain outcomes and highlight IFN-γ as a candidate biomarker to stratify patients at risk for chronic CHIKV-associated pain.

Discussion

In this study, we investigated the long-term consequences of chikungunya virus (CHIKV) infection on pain and joint pathology using a murine model that recapitulates both acute and chronic disease trajectories. CHIKV-infected mice developed mechanical allodynia, accompanied by joint inflammation, cartilage alterations, and detectable viral RNA in the infected joint, together with a sensory neuron stress signature. Rather than representing a uniform outcome of infection, stratification of CHIKV-infected mice into recovered and persistent groups revealed that a subset (~50%) exhibited long-lasting mechanical allodynia despite joint recovery and similar viral RNA levels, indicating that persistent pain is not directly explained by ongoing joint pathology or viral load. These findings mirror the clinical observation that, while most patients recover after the acute febrile phase, a significant fraction experience chronic arthralgia lasting month to years[3,5-8]. Our data are consistent with a model in which persistent-disease mice are distinguished by an IFN-γ-dominated immune profile, implicating this cytokine as a central component of neuroimmune pathways associated with pain persistence, beyond its established role in antiviral defense. Together, these results advance our understanding of how an acute CHIKV infection can transition into chronic pain and reframe persistent arthralgia as a consequence of maladaptive host responses rather than unresolved infection, suggesting new avenues for targeted immunomodulatory interventions.

In both patients and our mouse model, IFN-γ emerged as the most consistent correlate of persistent pain. Among the cytokines measured in our clinical cohort, only acute-phase IFN-γ levels predicted the subsequent development of chronic arthralgia, whereas TNF, IL-6, and IL-1β showed no association with long-term outcomes. ROC analysis confirmed that acute-phase IFN-γ possesses moderate-to-good discriminative power for identifying patients at risk of developing chronic arthralgia. This finding was mirrored in the experimental model, as mice with persistent pain displayed markedly higher systemic IFN-γ levels during the acute phase than recovered animals. Notably, although IFN-γ levels showed only a trend toward elevation during the chronic phase, they did not differ between outcome groups, indicating that persistent pain is not maintained by sustained systemic IFN-γ, but rather reflects the lasting impact of an exaggerated acute-phase response. These convergent clinical and experimental observations identify early IFN-γ responses as a key correlate of long-term pain susceptibility, extending earlier reports of elevated IFN-γ expression during CHIKV infection[19,21,23] Importantly, they highlight a dual role for IFN-γ, being indispensable for antiviral defence, but potentially priming maladaptive pain pathways when sustained or excessive[52]. Rather than contradicting its antiviral role, our data support a model in which exaggerated or temporally dysregulated IFN-γ responses during the acute phase imprint long-lasting neuroimmune alterations that persist after viral control, in line with prior studies linking IFN-γ to neuropathic pain[53,54].

Structural damage to cartilage and bone has been recognized as a major contributor to chronic arthralgia and joint dysfunction in both autoimmune arthritis, such as rheumatoid arthritis, and

degenerative joint diseases like osteoarthritis[55,56]. Although less studied, similar mechanisms may contribute to chronic joint pain following viral arthritis. Joint catabolism mediated by enzymes such as MMP13 and ADAMTS-4, along with an altered RANKL/OPG balance, are well-established drivers of long-term disability in rheumatoid arthritis and osteoarthritis models[33-36,57,58]. In the context of CHIKV infection, experimental studies have reported acute joint pathology, including proteoglycan loss, cartilage necrosis, and bone remodelling, supporting the idea that viral arthritis can involve early structural damage[59-61]. However, these investigations were largely limited to acute or subacute phases and did not assess long-term outcomes. By directly comparing recovered and persistent disease trajectories, our findings help clarify this issue, showing that although cartilage damage was evident during the acute phase, chronic pain persistence occurred independently of ongoing structural joint pathology. Together, these data argue against progressive joint degeneration as the primary driver of post-CHIKV chronic pain.

Persistent pain syndromes have emerged as an important component of the long-term sequelae following viral infections [62]. Consistently, a growing body of evidence indicates that diverse neurotropic and systemic viruses, including HIV, herpesviruses, SARS-CoV-2, and Zika virus, can trigger long-lasting sensory dysfunction and chronic neuropathic states through distinct pathogenic routes[63-69]. While some virus, such as varicella-zoster virus, can directly infect and damage sensory neurons[65,66], others including HIV[67] and Zika virus[68,69] cause neuronal dysfunction predominantly through indirect, immune-mediated mechanisms, in which pro-inflammatory cytokines and inflammatory mediators alter neuronal excitability and survival in the lack of overt viral cytopathicity [67,68,70]. Our findings place CHIKV firmly within this latter paradigm. The absence of detectable CHIKV RNA in dorsal root ganglia argues against direct viral persistence as the cause of sensory neuron injury, consistent with evidence that alphaviruses preferentially replicate in non-neuronal cells[71,72], particularly macrophages[20], while infection of mature neurons is restricted or attenuated[73,74]. Instead, the convergence of ATF3 induction, a canonical marker of neuronal stress, and the morphological abnormalities in the sciatic nerve fibers myelin indicates that neuronal injury arises downstream of sustained inflammatory signalling rather than viral tropism. Interestingly, we found myelin abnormalities and altered G-ratio in the sciatic nerves of the animals presenting persistent pain. Indeed, myelin injury has been related to allodynia and hyperalgesia even in the absence of neuronal lesion[75,76]. The absence of ATF3 induction at chronic stages likely reflects the transient nature of this stress response rather than neuronal recovery. In contrast, the persistent activation of cleaved caspase-3 observed in animals with chronic pain points to ongoing sublethal neuronal injury. While caspase-3 activation is classically associated with apoptotic cell death[50,77], evidence from nerve injury and chronic pain models indicates that sustained caspase-3 signalling can reflect ongoing sublethal neurodegenerative and plastic processes without overt neuronal loss death[78]. This interpretation aligns with observations in other viral models in which inflammatory mediators, rather than ongoing viral replication, drive long-term neuronal sensitization and persistent pain[63,79,80]. Collectively, these data support a model in which IFN-γ–driven neuro-immune interactions disrupt peripheral nerve homeostasis and predispose to chronic pain following CHIKV infection.

These findings align with emerging concepts that IFN-γ and related immune mediators can exert dual roles, being protective in pathogen clearance yet maladaptive when excessively or dysregulated during acute infection[52]. Sustained exposure of articular sensory nerve endings to inflammatory mediators may not only drive peripheral sensitization but also promote an injury-like sensory neuron state, contributing to neuropathic features of chronic joint pain[81-89]. Notably, pharmacological or genetic blockade of IFN-γ signalling prevented CHIKV-induced pain behaviours and abrogated markers of neuronal stress without affecting viral load, establishing a mechanistic dissociation between antiviral immunity and neuropathic pain. This distinction has direct translational relevance, as acute-phase IFN-γ responses may serve as a prognostic biomarker to identify patients at risk of developing chronic post-viral pain, while therapeutic targeting of IFN-γ or its downstream signalling could mitigate virus-induced chronic pain without compromising viral clearance.

More broadly, our work positions CHIKV-induced chronic arthralgia as a model to understand post-viral neuropathic pain, in which immune-mediated stress bridges acute infection and long-term dysfunction. Identifying IFN-γ as a key contributor to infection-associated neuronal stress and pain susceptibility provides a framework to investigate shared neuroimmune pathways across viral infections and to inform immunomodulatory interventions beyond CHIKV. Together, these insights not only advance our understanding of alphavirus pathogenesis but also underscore the broader principle that host antiviral responses can shape long-term neurological outcomes.

Acknowledgments

This work was supported by the Fundação de Amparo à Pesquisa do Estado do Rio de Janeiro (FAPERJ) (E-26/210.779/2021, E-26/210.075/2023, E-26/200.291/2025, E-26/2020.752/2019, E-26/010.000169/2020, SEI-260003/001141/2020, E-26/010.002260/2019), the Coordenação de Aperfeiçoamento de Pessoal de Nível Superior (CAPES) (88887.657702/2021-00), the Conselho Nacional de Desenvolvimento Científico e Tecnológico (CNPq) (312891/2018), the CAPES/STINT Brazil–Sweden Cooperation Program (88887.465506/2019-00), and the Fundação de Amparo à Pesquisa do Estado de São Paulo (FAPESP) (2024/22135-0). We thank João Batista Calixto and Marcelo Alves Mori for critical reading of the manuscript, and Ana Claudia Rangel, José Nilson dos Santos, Daiane Torres, and Bianca de Lima Almeida for technical support, including assistance with primary cell cultures.

STAR+METHODS

KEY RESOURCES TABLE

REAGENT or RESOURCE	SOURCE	IDENTIFIER
Antibodies		
Anti-mouse CD4 Monoclonal Antibody, FITC	Invitrogen	Cat# 11-0041-82
Anti-Mouse CD4 Monoclonal Antibody, PE	Invitrogen	Cat# 12-0042-82
Anti-mouse CD8a Monoclonal Antibody, APC	Invitrogen	Cat# 17-0081-82
Anti-mouse CD8a Monoclonal Antibody, eFluor™	Invitrogen	Cat# 48-0081-82
Anti-mouse CD11b Monoclonal Antibody, FITC	Invitrogen	Cat# 11-0112-82
Anti-mouse CD45 PerCP-Cy5	BioLegend	Cat# 103132
Anti-mouse CD45 Monoclonal Antibody, PE-Cy5	Invitrogen	Cat# 15-0451-81
FITC anti-mouse CD49b	BioLegend	Cat# 108905
APC anti-mouse IFN-γ Antibody	BioLegend	Cat# 505809
Biological samples		
Human Blood	Marcílio Dias Naval Hospital	N/A
Chemicals, peptides, and recombinant proteins		
Trizol	Invitrogen	Cat# 15596026

Fluoromount™	Electron Microscopy Sciences	Cat# 17984-25
eBioscience™ Brefeldin A	Invitrogen	Cat# 00-4506-51
eBioscience™ Cell Stimulation Cocktail	Invitrogen	Cat# 00-4970-93
Critical commercial assays		
High-Capacity cDNA Reverse Transcription Kit	Applied Biosystems	Cat# 4368813
Power SYBR Green Master Mix	Life Technologies	Cat# 4367659
TaqMan Universal PCR Master Mix	Applied Biosystems	Cat# 4304437
Mouse IFN-γ ELISA kit	R&D Systems	Cat# DY485-05
Human IL-1β/IL-1F2 Quantikine Elisa Kit	R&D Systems	Cat#DLB50
IFN-γ	R&D Systems	Cat. #485-MI/CF
MilliplexR MAP Kit High Sensitivity Magnetic Bead Cytokine Panel for TNF-α, IL-6	Merck	Cat# HCYTA-60K
Oligonucleotides		
Primers for qPCR, see supplementary table 1	This paper	N/A
Software and algorithms		
ImageJ v1.53	NIH	https://imagej.nih.gov/ij/
FlowJo™ software	BD Biosciences	https://www.flowjo.com/
Prism v10.	GraphPad	https://www.graphpad.com/

RESOURCE AVAILABILITY

Lead contact

Further information and requests for resources, materials, or reagents should be directed to the corresponding authors, Cláudia P. Figueiredo (claudia@pharma.ufrj.br) and Robson da Costa (rbsncosta@farmacia.ufrj.br).

Materials availability

This study did not generate new unique reagents.

Data and code availability

- The original data within the paper will be available from the lead contact upon request.
- This paper does not report original code.
- Any additional information in this paper is available from the lead contact upon requests.

EXPERIMENTAL MODEL AND SUBJECT DETAILS

Animals

Adult male and female Swiss mice were used in most experiments. In some experiments, C57BL/6J wild-type (WT) and *Ifng*$^{-/-}$ mice[90] were used. All mice were 8–12 weeks old. Animals were housed in groups of five per cage with free access to food and water, under a 12 h light/dark cycle, with controlled temperature and humidity. All procedures followed the ‘‘Principles of Laboratory Animal Care’’ (US National Institutes of Health) and were approved by the Institutional Animal Care and Use Committee of the Federal University of Rio de Janeiro, Brazil (protocol number A19/24-008-21).

Viruses

CHIKV was isolated from a febrile Brazilian patient during the 2016 outbreak, and viral stocks were generated as previously described[91]. To generate CHIKV stock, C6/36 cells were infected at a multiplicity of infection (MOI) of 0.01. After 30 hours of infection, the culture supernatant was then collected and clarified by centrifugation at 2.000 rpm for 10 min. Clarified supernatants were aliquoted and stored at −80°C. Viral titers of the resulting stocks were determined by plaque assay in Vero cells.

Chikungunya Virus (CHIKV) Inoculation

Mice were anesthetized with isoflurane and inoculated intra-articularly (i.a.) in the left knee joint with 10 µL of CHIKV (strain BHI3768; 10^6 PFU). Control animals received an equivalent volume of virus-free C6/36 medium (Mock).

RNA Extraction and qPCR

Total RNA was extracted from knee joints and DRG using TRIzol Reagent (Invitrogen), according to the manufacturer's instructions. RNA concentration and purity were assessed using a Thermo Scientific NanoDrop spectrophotometer by measuring absorbance ratios at 260/280 and 260/230 nm. Only preparations with absorbance ratios ≥1.8 were used. 1µg of isolated RNA was reverse-transcribed using the High-Capacity cDNA Reverse Transcription Kit (Thermo Fisher Scientific Inc). Quantitative PCR was performed using Power SYBR Green PCR Master Mix (Life Technologies) on a QuantStudio 3 Real-Time PCR System (Thermo Fisher Scientific). Gene expression was quantified using the ΔΔCt method and normalized to β-Actin. Target genes included inflammatory and matrix remodeling markers (*Tnf, Il6, Ifng, Ifna, Ifnb, Mmp13, Adamts4, Rankl, Opg)* and neuronal stress markers such as *atf3*. Viral load detection was performed using the TaqMan Mix kit (Thermo Fisher Scientific) following the manufacturer's protocol, employing primers specific for the CHIKV nsp1 gene (Supplementary Table 2). Primer sequences for all targets are listed in Supplementary Table 1.

Viral Plaque Assay

Viral titers were quantified by plaque formation assay. Tissues were weighed and homogenized in DMEM supplemented with penicillin and streptomycin at a ratio of 0.2 mg tissue/µL sample (w/v). After homogenization, 25 µL of each sample was serially diluted in serum-free DMEM High Glucose. Semi-confluent Vero cells seeded in 24-well plates were inoculated with 200 µL of each dilution (10^{-1} to 10^{-6}) and incubated for 1 h at 37°C with 5% CO_2. Following adsorption, wells were overlaid with 1 mL of DMEM containing 1% carboxymethylcellulose, 1% FBS, and 1% penicillin/streptomycin and incubated for 40 h under standard culture conditions. Cells were then fixed with 10% formaldehyde for 1 h, washed, and stained with 1% crystal violet in 20% ethanol for 20 min. Plaques were counted and titers expressed as plaque-forming units (PFU).

Immunohistochemistry for dsRNA

Knee joints were fixed in 4% paraformaldehyde, decalcified in EDTA, embedded in paraffin, and sectioned sagittally at 5 µm. Sections were deparaffinized, rehydrated, and subjected to antigen retrieval in citrate buffer (pH 6.0) for 30 min at 95–98 °C. Tissue permeabilization was performed with 0.5% Triton X-100 for 30 min, followed by blocking in 0.2% Triton X-100, 3% BSA, and 5% normal goat serum (NGS) for 2 h at room temperature. Primary antibodies against dsRNA (clone J2; Nordic-MUbio) were diluted in Primary Antibody Diluent and applied overnight at 4 °C. After washing, sections were incubated with Alexa Fluor™ 488 goat anti-mouse IgG secondary antibody (Invitrogen) for 1 h at room temperature. Nuclei were counterstained with DAPI, and slides were mounted with fluorescence mounting medium for imaging.

Pain Sensitivity Assessment

Mechanical sensitivity was assessed using calibrated von Frey filaments (0.07–2.0 g) applied to the plantar surface of the ipsilateral hind paw[92]. Paw withdrawal thresholds were determined using the up-and-down method [93]. Cold sensitivity was evaluated by applying a drop of acetone (approximately 50 µL) to the plantar surface, and the duration of nocifensive behaviours (shaking, licking, or lifting of the paw) was recorded over 60 seconds[94]. Mice were habituated to the testing environment for at least 1 hour before each session. All evaluations were performed at baseline and at defined time points post-infection by experimenters blinded to experimental groups.

Histology and Cartilage Damage Scoring

Knee joints were harvested, fixed in 4% paraformaldehyde, decalcified in EDTA, and embedded in paraffin. Serial sagittal sections (5 µm) were stained with hematoxylin and eosin (H&E), safranin-O/fast green, or toluidine blue using standard protocols. Cartilage pathology in H&E-stained sections was scored by two independent blinded observers, as previously described[95]. For safranin-O/fast green and toluidine blue staining, cartilage matrix content was quantified using ImageJ software by measuring the stained area and intensity relative to total cartilage area in defined regions of interest (ROIs).

Flow cytometry

Mock and infected mice were anesthetized with ketamine/xylazine and subjected to two consecutive intra-articular lavages of the knee using 10 µL of PBS supplemented with 5% FBS. Synovial fluid samples were stained with fluorochrome-conjugated monoclonal antibodies to identify T cells and phagocytes. The following antibodies were used: anti-CD4 PE (eBioscience), anti-CD8 APC (eBioscience), anti-CD11b FITC (eBioscience), and anti-CD45 PE-Cy5 (eBioscience). Samples were incubated with the antibody mixture for 30 min at room temperature in the dark, washed with PBS containing 5% FBS, and resuspended in a staining buffer. Flow cytometric acquisition was performed using a FACS Canto™ cytometer (BD Biosciences), and data were analyzed with FlowJo™ software (BD Biosciences). Compensation was performed using single-stained controls for each fluorochrome. The gating strategy included exclusion of doublets based on FSC-A versus FSC-H, followed by selection of live cells using FSC versus SSC parameters. Among live cells, $CD45^+$ leukocytes were gated and further classified into $CD4^+$ T cells, $CD8^+$ T cells, and phagocytes ($CD11b^+$).

Intracellular IFN-γ Detection by Flow Cytometry

Mock and infected mice were anesthetized with ketamine/xylazine and subjected to two consecutive intra-articular lavages of the knee using 10 µL of PBS supplemented with 5% FBS. Synovial fluid cells were stimulated with Cell Stimulation Cocktail (eBioscience) for 3h, in the presence of brefeldin A to block cytokine secretion. Cells were then stained for surface markers using anti-CD4 PE (eBioscience), anti-CD8 eFluor450 (eBioscience), anti-CD45 PE-Cy5 (eBioscience), and anti-CD49b FITC (eBioscience). After surface labeling, cells were fixed and permeabilized with the BD Cytofix/Cytoperm™ kit (BD Biosciences) and stained intracellularly with anti–IFN-γ APC (eBioscience). Samples were washed, resuspended in PBS, and acquired on a BD FACSCanto™ flow cytometer. Data were analyzed with FlowJo software (BD Biosciences).

Gating Strategy

Doublets were excluded by FSC-A × FSC-H. Live cells were selected based on FSC × SSC, followed by gating on $CD45^+$ leukocytes. These were subdivided into $CD4^+$, $CD8^+$, and $CD49b^+$ populations, and IFN-γ expression was quantified within each subset.

Intra-articular injection of recombinant IFN-γ

Recombinant murine interferon-gamma (IFN-γ; [R&D Systems, Cat. #485-MI/CF]) was administered i.a. into the left knee joint of naïve mice at a dose of 300 U/site every 48 hours over a 7-day period. This

dosing regimen was selected based on preliminary titration experiments showing that a higher dose (600 U/site) did not produce additional effects compared with the 300 U dose, and was consistent with intra-articular doses previously used for other recombinant cytokines in the literature[96,97]. Mechanical sensitivity was assessed using calibrated von Frey filaments, as described above.

DRG neuron culture and stimulation

Primary dorsal root ganglion (DRG) neurons were isolated from adult mice and cultured for 24 h following a previously described protocol[98]. Cells were then stimulated with recombinant IFN-γ (1 ng/mL or 8,4 U/mL; R&D Systems, Cat. #485-MI/CF) or capsaicin (1 µM, positive control) for 60 minutes. Neurons were fixed and immunostained for p-ERK (Anti-p-ERK, Cell Signaling, cat. 4370S), ATF3 (Anti-ATF3, NovusBio, cat. NBP1-02935), and NeuN (Anti-NeuN, Cell Signaling, Cat. 24307S). Confocal images were acquired to quantify the percentage of marker-positive neurons. In parallel, *Atf3* mRNA expression was assessed by RT-qPCR.

IFN-γ receptor blockade

Pharmacological inhibition of IFN-γ signalling was achieved via intra-articular administration of a monoclonal anti-IFN-γ receptor antibody (anti-CD119; clone GR-20, Bio X Cell, Cat# BE0245). The antibody was injected at 0.5 and 5 µg/site[99,100] into the left knee joint at the time of infection and subsequently every 48 hours for a total of 4doses. Control animals received an equivalent amount of isotype-matched IgG (Bio X Cell, Cat# BE0091). In parallel, $Ifng^{-/-}$ mice[90] were used to genetically validate the role of IFN-γ signalling in CHIKV-induced responses.

IFN-γ quantification

Systemic levels of IFN-γ were measured in mouse serum samples collected at defined time points using a commercially available ELISA kit (R&D Systems, Cat: DY485-05), following the manufacturer's instructions. Samples were run in triplicate, and cytokine concentrations were calculated based on standard curves generated in each plate.

Semithin Section Preparation and Morphometric Analysis

Semithin nerve analyses were performed as previously described[101]. Transverse semithin sections (300–500 nm) were collected on glass slides, stained with toluidine blue, and imaged at 100× magnification using a light microscope equipped with a digital camera. Qualitative and quantitative assessments of myelinated fibers were performed along the length of each nerve. For morphometric analysis, five fields per nerve were acquired at 100× magnification to quantify myelin abnormalities and G-ratio. Additionally, panoramic images were generated from 40× micrographs of each nerve using Adobe Photoshop CS6, and the total number of myelinated fibers was quantified.

NF200 Immunostaining of the Sciatic Nerve

Dissected sciatic nerves were fixed in 4% paraformaldehyde for 24 h, washed in PBS (pH 7.4) for 24 h, and cryoprotected in 10%, 20%, and 30% sucrose solutions (48–72 h each). Tissues were embedded, flash-frozen in liquid nitrogen, and sectioned transversely at 12 µm using a cryostat (Leica CM1850). Sections were washed twice in 0.3% PBST and incubated in a blocking solution (PBS containing 0.3% Triton X-100 and 10% normal goat serum) for 1 h at room temperature. Samples were then incubated with the primary antibody anti-NF200 (1:1000; Sigma) for 24 hours at 4 °C. After PBS washes, sections were incubated with Alexa Fluor™ 488 goat anti-mouse IgG (1:500; Molecular Probes) for 2 h at room temperature, washed, and counterstained with DAPI (Sigma). Slides were mounted with Fluoromount™ (Electron Microscopy Sciences, Cat# 17984-25) and stored at −20 °C. Omission of the primary antibody served as a negative control. Fluorescence images were acquired on a Zeiss microscope using a 20× objective. The images were

processed and analyzed using Fiji (ImageJ). Mean fluorescence intensity was measured by selecting regions of interest (ROIs) and using the Analyze > Measure function to record the Mean Gray Value of NF200 immunoreactivity.

Cleaved Caspase-3 Immunostaining of the Dorsal Root Ganglion

Dissected DRGs were fixed in 4% paraformaldehyde for 24 h, washed in PBS (pH 7.4) for 24 h, and cryoprotected in 10%, 20%, and 30% sucrose solutions (48–72 h each). Tissues were embedded, flash-frozen in liquid nitrogen, and sectioned transversely at 12 µm using a cryostat (Leica CM1850). Sections were washed twice in 0.3% PBST and incubated in a blocking solution (PBS containing 0.3% Triton X-100 and 10% normal goat serum) for 1 h at room temperature. Samples were then incubated with the primary antibody anti-cleaved caspase-3 (1:1000; Cell signalling Cat: #9661S) for 24 hours at 4 °C. After PBS washes, sections were incubated with Alexa FluorTM 488 goat anti-mouse IgG (1:500; Molecular Probes) for 2 h at room temperature, washed, and counterstained with DAPI (Sigma). Slides were mounted with Fluoromount™ (Electron Microscopy Sciences, Cat# 17984-25) and stored at −20 °C. Omission of the primary antibody served as a negative control. Fluorescence images were acquired on a Zeiss microscope using a 20× objective. The images were processed and analyzed using Fiji (ImageJ). Mean fluorescence intensity was measured by selecting regions of interest (ROIs) and using the Analyze > Measure function to record the Mean Gray Value of cleaved caspase-3 immunoreactivity.

Electron microscopy

Sciatic nerves were fixed in 2.5% glutaraldehyde diluted in 0.1 M cacodylate buffer for 24 hours, washed, and post-fixed for 2 hours in 1% osmium tetroxide containing 0.8% potassium ferrocyanide in 0.1 M cacodylate buffer (pH 7.4). Following, samples were washed and dehydrated in acetone graded series before being embedded in increasing concentration of Spurr. Spurr-embedded samples were hardened at 60°C for 72 h and 80-nm ultrathin sections were prepared and attached to copper grids. Lead citrate and uranyl acetate were used for post-staining, and samples were observed with a transmission electron microscope (HITACHI HT 7800).

Clinical cohort and cytokine analysis

A retrospective cohort of individuals exposed to CHIKV during the epidemic period in Rio de Janeiro, Brazil (2018–2019), was analysed. Fifty participants of both sexes, aged over 18 years, and with laboratory-confirmed CHIKV infection were included in the study. Individuals with a history of chronic pain were excluded. Participants were followed up using a structured questionnaire to assess the incidence of chronic arthralgia (joint pain lasting ≥3 months after diagnosis) and its association with joint pain characteristics during the acute phase, as well as levels of inflammatory markers TNF-α, IL-6, IL-1β, and IFN-γ in serum samples collected at diagnosis and quantified using enzyme-linked immunosorbent assay (ELISA) according to the manufacturer's instructions. All procedures were approved by the local institutional ethics committee (protocol number 42340920.7.0000.5259), and written informed consent was obtained from all participants.

Statistical Analysis

Data are presented as mean ± SEM. Group comparisons were performed using two-tailed unpaired t-tests, one- or two-way ANOVA with appropriate post hoc tests, or non-parametric equivalents when required. Statistical significance was set at $P < 0.05$. All analyses were conducted using GraphPad Prism v10.

Figure Legends:

Figure 1. CHIKV infection drives joint pathology and transient neuronal stress responses.
(A) Schematic of intra-articular (i.a.) CHIKV (10^6 PFU) inoculation into the mouse knee joint.

(B) CHIKV RNA levels in ipsilateral (dark blue) and contralateral (gray) knee joints were quantified by qPCR over time. Viral RNA peaked at 1 dpi in the ipsilateral joint and remained detectable up to 28 dpi.

(C) Infectious CHIKV particles in ipsilateral knee joints were quantified by plaque assay over time. Viral titers peaked at 1 dpi and declined to undetectable levels by 3 dpi.

(D-G) Localization of CHIKV RNA in knee joints. Sections were stained with anti-dsRNA antibody (green). **(D)** Mock controls showed no signal. **(E)** CHIKV-infected knees at 7 dpi displayed strong dsRNA immunoreactivity. Higher magnification revealed viral RNA in **(F)** articular cartilage and **(G)** synovial tissue.

(H) Time course of paw withdrawal thresholds (PWT, g) to von Frey stimulation in Mock- and CHIKV-inoculated mice (0–28 dpi). CHIKV significantly reduced PWT compared with Mock at multiple time points. Data are mean ± SEM. Two-way ANOVA with Sidak's multiple-comparisons test, $P < 0.05$; n = 15-17 per group.

(I) Area under the curve (AUC) of PWT from panel H. AUC was significantly lower in CHIKV mice. Two-tailed unpaired *t* test; $P < 0.0001$; n = 15–17 per group.

(J) Time course of cold sensitivity in Mock- and CHIKV-inoculated mice (0–28 dpi), assessed by the acetone test. CHIKV infection did not alter cold nocifensive responses compared with Mock. Data are mean ± SEM. Two-way ANOVA; n.s.; n = 15-17 per group.

(K) Area under the curve (AUC) of cold nocifensive responses from panel J. No significant differences were detected between Mock and CHIKV groups. Data are mean ± SEM. Two-tailed unpaired *t* test; n.s.; n = 15-17 per group.

(L–M) Representative Safranin-O-stained sections of knee joint cartilage from Mock and CHIKV-inoculated mice at 28 dpi, showing reduced proteoglycan content in infected joints. **(N)** Quantification of Safranin-O-positive staining reveals reduced cartilage proteoglycan content in CHIKV-infected knees at 28 dpi. **(O)** Quantification of toluidine blue staining demonstrates a significant decrease in proteoglycan content in CHIKV-infected joints at 28 dpi. For panels N and O, data are mean ± SEM. Two-tailed unpaired t tests in **(A)** $P = 0.048$ and **(B)** $P = 0.004$; n = 5-7 mice per group.

(P–R) CHIKV infection upregulates joint catabolic gene expression at 28 dpi. qPCR analysis of ipsilateral knee tissue shows significant increases in Mmp13, Adamts4, and the Rankl/Opg mRNA ratio in CHIKV-infected mice compared with Mock controls. Data are mean ± SEM. Two-tailed unpaired *t* test in **(P)** $P = 0.003$, **(Q)** $P = 0.002$ and **(R)** $P = 0.010$. **(P, Q)** n = 9 mice per group and **(R)** n = 4–5 mice per group.

(S) Quantification of *Atf3* mRNA expression in dorsal root ganglia (DRG) at 7 and 28 dpi. CHIKV infection induced a marked upregulation of *Atf3* transcripts at 28 dpi compared with mock-infected controls. One-way ANOVA followed by Tukey's post hoc test, $P < 0.0001$; n = 3-5 per group.

(T) Viral RNA levels in the DRG at 4 h to 7 dpi. CHIKV RNA was undetectable except for a single low-level detection at 3 dpi, consistent with minimal viral persistence. One-way ANOVA followed by Tukey's post hoc test, n.s.; n = 3-6 per group.

Figure 2. Sustained IFN-γ response and T cell recruitment underlie joint inflammation after CHIKV infection.

(A–E) qPCR analysis of pro-inflammatory mediators in ipsilateral knee joints after intra-articular CHIKV infection. *Tnf* **(A)** and ***Il6*** **(B)** were transiently induced, peaking at 7 and 3 dpi, respectively. Type I interferons (*Ifna*, C; *Ifnb*, D) peaked at 1 dpi and returned to baseline thereafter. In contrast, *Ifng* **(E)** was strongly upregulated, peaking at 7 dpi and remaining elevated through at least 28 dpi. One-way ANOVA followed by Tukey's post hoc test in **(A)** $P = 0.032$, **(B)** $P = 0.0186$, **(C)** #$P = 0.065$, **(D)** $P = 0.026$ and **(E)** $P = 0.022$; n = 3-6 per group.

(F–H) Flow cytometry analysis of synovial fluid shows marked T cell accumulation after CHIKV infection. **(F)** Representative plots of $CD4^+$ and $CD8^+$ T cells in Mock, 7 dpi, and 28 dpi joints. Quantification revealed significant increases in $CD4^+$ **(G)** and $CD8^+$ **(H)** T cells at 7 dpi, which declined by 28 dpi but remained above Mock levels. One-way ANOVA followed by Dunnett's post hoc test in **(G)** $P < 0.0001$ and **(H)** $P = 0.005$; n = 3–4 animals per group.

(I–K) Flow cytometry analysis of $CD11b^+CD45^+$ myeloid cells. (I) Representative plots of synovial fluid from Mock, 7 dpi, and 28 dpi animals. **(J)** Quantification showed a strong increase in $CD11b^+CD45^+$ cells in joint fluid at 7 dpi, which declined toward baseline by 28 dpi. **(K)** In parallel, the frequency of circulating $CD11b^+CD45^+$ cells in blood was significantly reduced at 7 dpi, consistent with migration into the joint. One-way ANOVA followed by Dunnett's post hoc test in **(J)** $P = 0.027$ and **(K)** $P = 0.018$; n = 4 animals per group.

(L–O) Flow cytometry analysis of IFN-γ–producing T cells in the synovial fluid after CHIKV infection. **(L, N)** Representative plots of IFN-γ expression in $CD8^+$ **(L)** and $CD4^+$ **(N)** T cells from Mock, 7 dpi, and 28 dpi joints. **(M)** Quantification revealed a marked increase in the frequency of IFN-γ^+ $CD8^+$ T cells at 7 dpi, which was markedly reduced by 28 dpi. **(O)** A similar but less pronounced increase was observed in IFN-γ^+ $CD4^+$ T cells at 7 dpi. One-way ANOVA followed by Dunnett's post hoc test in **(M)** $P < 0.0001$ and **(O)** $P = 0.004$; n = 3–4 animals per group.

Figure 3. IFN-γ drives CHIKV-induced pain and neuronal stress.

(A–B) Intra-articular (i.a.) injections of IFN-γ (300 U or 600U/site; days 0, 2 and 4) induced a rapid and persistent reduction in paw withdrawal thresholds compared with saline, as shown by the time course **(A)** and AUC analysis **(B)**, demonstrating robust mechanical allodynia. Two-way ANOVA followed by Tukey's post hoc test in **(A)** $P < 0.05$ and One-way ANOVA followed by Tukey's post hoc test in **(B)** $P < 0.001$; n = 9–14 animals per group.

(C–E) IFN-γ did not alter Adamts4 **(C)** or Mmp13 **(D)** expression in the joint but markedly increased *Atf3* mRNA levels in dorsal root ganglia (DRG; E), consistent with a neuronal stress response independent of joint catabolism. Two-tailed unpaired *t* test in **(C)** n.s., **(D)** n.s., **(E)** $P = 0.047$; n = 7-9 animals per group.

(F–H) IFN-γ directly activates cultured DRG neurons following 1 h exposure (1 ng/mL). **(F)** Representative double immunostaining for NeuN (red), p-ERK (green), and DAPI (blue). **(G)** Quantification of p-ERK mean

fluorescence intensity in NeuN$^+$ neurons, showing enhanced neuronal activation following IFN-γ treatment. **(H)** Capsaicin (0.5 µg, 5 min), used as a positive control, similarly increased p-ERK immunoreactivity. Quantifications were performed in three independent cultures, with two coverslips per culture; fluorescence intensity was measured at the single-cell level in NeuN$^+$ neurons. Each data point represents one cell. Statistical analysis was performed using two-tailed unpaired *t* test; **(G)** $P < 0.0001$; **(H)** $P = 0.0056$.

(I–K) IFN-γ also induced ATF3 expression in cultured DRG neurons. **(I)** Representative double immunostaining for NeuN (red), ATF3 (green), and DAPI (blue). **(J)** Quantification of ATF3 mean fluorescence intensity in NeuN$^+$ neurons. **(K)** qPCR confirmed upregulation of *Atf3* mRNA following IFN-γ exposure. Quantifications were performed in three independent cultures, with two coverslips per culture; fluorescence intensity was measured at the single-cell level in NeuN$^+$ neurons. Each data point represents one cell. Two-tailed unpaired *t* test in **(J)** $P = 0.0011$ and **(K)** $P = 0.0033$.

(L–U) Pharmacological or genetic blockade of IFN-γ signaling prevents CHIKV-induced pain and neuronal stress without altering viral load. **(L)** Anti-CD119 (IFN-γR1) monoclonal antibody prevented CHIKV-induced mechanical allodynia, as shown by time course **(L)** and AUC **(M)** analyses. Two-way ANOVA followed by Tukey's multiple-comparisons test in **(L)** $P < 0.0001$; One-way ANOVA followed by Tukey's post hoc test in **(M)** $P = 0.0017$; n = 8 animals per group.

(N) Anti-CD119 treatment did not alter viral RNA levels in the joint, indicating that pharmacological IFN-γ blockade alleviates pain without impacting local viral burden. Two-tailed unpaired *t* test, n.s.; n = 7-8 animals per group

(O, P) Anti-CD119 treatment attenuated CHIKV-induced upregulation of Adamts4 (O) and Mmp13 **(P)** in the joint, indicating that while IFN-γ alone is insufficient to drive catabolic gene expression, its signaling contributes to maintaining joint-destructive responses in the context of CHIKV infection. One-way ANOVA followed by Tukey's post hoc test in **(O)** $P = 0.002$ and **(P)** $P = 0.001$; n = 5-7 animals per group.

(Q–T) Similarly, IFN-γ receptor-deficient (Ifngr1^{-}/$^{-}$) mice were protected from CHIKV-induced mechanical allodynia **(Q, R)** and exhibited abolished *Adamts4* **(S)** and *Mmp13* **(T)** induction, with no change in joint viral RNA burden. **(U)** *Atf3* mRNA upregulation in DRG observed in WT animals was absent in Ifngr1^{-}/$^{-}$ mice, demonstrating that IFN-γ signaling is essential for CHIKV-induced neuronal stress and pain persistence. Two-way ANOVA followed by Tukey's multiple-comparisons test in **(Q)** $P < 0.05$; **(R-U)** One-way ANOVA followed by Tukey's post hoc test in **(R)** $P = 0.003$, **(S)** $P = 0.043$, **(T)** $P = 0.003$ and **(U)** $P = 0.015$. n = 8 animals per group.

Figure 4. Distinct pain outcomes after CHIKV infection are associated with elevated IFN-γ responses and peripheral nerve pathology.

(A) Schematic representation of intra-articular (i.a.) CHIKV (10^6 PFU) inoculation into the mouse knee joint.

(B) Time course of paw withdrawal thresholds (PWT, g) to von Frey stimulation in Mock- and CHIKV-inoculated mice (0–77 dpi). CHIKV lowered PWT compared with Mock. Two-way ANOVA followed by Tukey's post hoc test, $P < 0.05$. n = 9-24 animals per group.

(C) Area under the curve (AUC) of PWT from panel B. AUC was significantly lower in CHIKV mice. Two-tailed unpaired *t* test, $P < 0.0001$. n = 9-24 animals per group.

(D) CHIKV-infected mice were stratified at 77 dpi by mechanical sensitivity: ≥30 % reduction in PWT defined persistent (CHIKV-Persis., orange circles) and <30 % defined recovered (CHIKV-Recov., blue circles) groups. This classification revealed two distinct pain phenotypes in CHIKV-infected mice.

(E) Time course of PWT (% baseline) in CHIKV-infected mice stratified at 77 dpi as demonstrated in D. CHIKV-Persis. mice maintained significantly lower PWT during the late phase (42-77 dpi) when compared with CHIKV-Recov. group. Two-way ANOVA with Tukey's multiple-comparisons test, $P < 0.05$. n = 9-13 animals per group.

(F) AUC (42-77 dpi) of PWT from panel E. AUC was significantly lower in CHIKV-Persis. group. One-way ANOVA with Tukey's post hoc test, $P = 0.043$ (CHIKV-Recov. vs. CHIKV-Persis.); n = 9-13 animals per group.

(G, H) Quantification of CHIKV RNA (Eq. PFU/µg RNA) in knee joints **(G)** and DRG **(H)** from CHIKV-Persis., CHIKV-Recov., and Mock groups at 77 dpi. Joint viral loads did not differ between groups, and viral RNA was undetectable in DRG, suggesting that persistent pain is independent of viral persistence. Two-tailed unpaired *t* tests in **(G)** and **(H);** n.s. n = 5-9 animals per group.

(I-K) Levels of catabolic genes in knee joints of CHIKV-Recov. and CHIKV-Persis. mice at 77 dpi. *Mmp13* **(I)** and *Adamts4* **(J)** levels, and the Rankl/Opg mRNA ratio (**K)** did not differ between groups. Two-tailed unpaired *t* tests in **(I)**, **(J)** and **(K)**, n.s. n = 7-11 animals per group.

(L, M) Serum IFN-γ concentrations were elevated in CHIKV-Persis. mice during the acute phase, but not during the chronic phase of infection. **(L)** At 7 dpi (acute phase), IFN-γ levels were significantly higher in CHIKV-Persis. animals compared with Mock and CHIKV-Recov. groups. One-way ANOVA followed with Tukey's post hoc test in **(L)** $P = 0.023$ (Mock vs. CHIKV-Persis.); in **(M)** n.s.. n = 6-7 animals per group.

Figure 5. Persistent pain after CHIKV infection is associated with caspase-3 activation in dorsal root ganglia (DRG) and structural abnormalities in peripheral myelinated fibers.
(A) Representative images of lumbar DRG immunostained for cleaved caspase-3 from Mock, Recovered (CHIKV-Recov.), and Persistent (CHIKV-Persis.) mice at 77 dpi. Cleaved caspase-3–positive cells are markedly increased in mice with persistent pain.

(B) Quantification of cleaved caspase-3 immunoreactivity in DRG shows a significant increase in the CHIKV-Persis. group compared with Mock and CHIKV-Recov. mice, indicating ongoing neuronal injury selectively associated with long-term pain. One-way ANOVA followed with Tukey's post hoc test, $P = 0.041$ (Mock vs. CHIKV-Persis.). n = 4 animals per group.

(C) Representative semithin transverse sciatic nerve sections stained with toluidine blue showing comparable myelinated fiber density across groups (see quantification in Figure S4B).

(D-E) CHIKV-Persis. mice exhibit increased myelin irregularities, whereas overall myelinated fiber density is comparable across groups. **(D)** Myelin infoldings and **(E)** myelin splitting events are increased in CHIKV-Persis. mice. One-way ANOVA with Tukey's post hoc test. $P = 0.038$. n = 3-5 animals per group.

(F) G-ratio distribution shows a marked reduction in the proportion of fibers within the 0.56–0.65 range in CHIKV-Persis. mice, compared with Mock and CHIKV-Recov. groups. Two-way ANOVA with Tukey's post hoc test. $P = 0.045$ (CHIKV-Persis. vs. CHIKV-Recov.). n = 4–5 animals per group.

(G) Transmission electron microscopy of sciatic nerves at 77 dpi. Mock and CHIKV-Recov. animals display compact, concentrically arranged myelin lamellae with uniform periodicity and preserved axonal morphology. exhibit pronounced myelin pathology, including extensive lamellar separation and decompaction, accumulation of electron-dense fibrillar material within split lamellae, and focal myelin unraveling with loss of circular geometry.

Figure 6. IFN-γ elevation underlies chronic pain after CHIKV infection.
(A) Cohort of patients with confirmed CHIKV infection, with blood collected during the acute phase and clinical classification 3 months later as recovered (CHIKV-Recov., n = 20) or with persistent arthralgia (CHIKV-Chronic, n = 22).

(B) Forest plot showing odds ratios (ORs) and 95% confidence intervals (CIs) for acute-phase clinical symptoms comparing patients who developed chronic arthralgia versus those who recovered 3 months after CHIKV infection. No symptom showed a significant association with chronic outcome.

(C, E, G, I) Serum TNF-α (C), IL-6 (E), IL-1β (G), and IFN-γ (I) levels measured during the acute phase in CHIKV-Recov. and CHIKV-Chronic patients. IFN-γ levels were significantly higher in CHIKV-Chronic patients. Two-tailed unpaired t tests: TNF-α, IL-6, and IL-1β, n.s.; IFN-γ, $P = 0.011$. $n = 14–22$ per group.

(D, F, H, J) Receiver operating characteristic (ROC) analyses corresponding to TNF-α (D), IL-6 (F), IL-1β (H), and IFN-γ (J). IFN-γ showed the highest discriminative performance for chronic arthralgia (area under the curve, AUC = 0,73), whereas TNF-α, IL-6, and IL-1β displayed limited predictive value (AUCs = 0.52–0.66). Sample size per group ranged from n = 14 to 22.

Supplementary Figures Legends:

Figure S1. CHIKV infection induces mechanical and cold allodynia in male and female mice.
(A–D) Time course of paw withdrawal thresholds (PWT, g) to von Frey stimulation in Mock- and CHIKV-inoculated mice (0-28 dpi) **(A)** Female mice; **(B)** area under the curve (AUC) corresponding to panel A; **(C)** male mice; and **(D)** AUC corresponding to panel C. CHIKV infection significantly reduced PWT compared with Mock at multiple time points in both sexes. Data are presented as mean ± SEM. Two-way ANOVA with Sidak's multiple-comparisons test, $P < 0.05$. $n = 7–9$ animals per group.

(E–H) Time course of cold nocifensive responses (s) to acetone stimulation in Mock- and CHIKV-inoculated mice (0-28 dpi). **(E)** Female mice; **(F)** AUC corresponding to panel E; **(G)** male mice; and **(H)** AUC corresponding to panel G. Only CHIKV-infected female mice exhibited increased cold nocifensive responses. Data are presented as mean ± SEM. Two-way ANOVA with Sidak's multiple-comparisons test in (E) and (G), n.s. Two-tailed unpaired *t* test in **(F)**, $P = 0.0009$, and **(H)**, n.s. $n = 7–9$ animals per group.

Figure S2. Immune cell infiltration, cartilage integrity, and pharmacological modulation of mechanical allodynia after CHIKV infection

(A–D) Immune cell infiltration in the infected joint. Representative images and quantification of immune cell infiltrates in the articular region at 7 and 28 dpi show robust inflammation at 7 dpi **(C)**, with persistent

immune cell presence at 28 dpi **(D)**. Two-tailed unpaired *t* test in **(C)** $P = 0.005$ and **(D)** $P = 0.028$. $n = 5$-8 animals per group.

(E, F) Toluidine blue staining of knee joint sections reveals cartilage alterations following CHIKV infection. Representative images and quantitative analysis (see Figure 1O) indicate increased cartilage damage in infected animals compared with Mock controls.

(G, H) Effect of gabapentin treatment on CHIKV-induced mechanical allodynia at 28 dpi. **(G)** Time course of paw withdrawal thresholds (PWT, g) to von Frey stimulation in CHIKV-infected mice following gabapentin administration (p.o., 100 mg/kg). **(H)** Area under the curve (AUC) analysis. A single dose of gabapentin attenuates mechanical allodynia in CHIKV-infected mice. Two-way ANOVA with Sidak's multiple-comparisons test in **(G)**, $P < 0.05$; two-tailed unpaired *t* test in **(H),** $P = 0.017$. $n = 9$ animals per group.

Figure S3.NK cell–derived IFN-γ, IFN-γ receptor blockade, and viral load in DRG after CHIKV infection

(A, B) Flow cytometry analysis of IFN-γ–producing NK cells in the synovial fluid of the infected knee joint at 7 and 28 dpi. **(A)** Representative gating strategy and plots; **(B)** quantification of IFN-γ–secreting NK cells. One-way ANOVA with Tukey's multiple-comparisons test; n.s. n = 4 animals per group.

(C) Effect of intra-articular blockade of IFN-γ signaling on CHIKV-induced mechanical allodynia. Paw withdrawal thresholds (PTW, g) measured by von Frey testing show that intra-articular administration of an anti-CD119 antibody (5 µg/site or 0.5 µg/site) attenuates mechanical allodynia, with the 5 µg dose showing greater efficacy. Two-way ANOVA with Tukey's multiple-comparisons test; $P < 0.05$. n = 8–9 animals per group.

(D) CHIKV RNA levels in dorsal root ganglia (DRG) from IFN-γ–deficient (*Ifng*$^{-}$/$^{-}$) mice. No differences in viral load were detected between groups, indicating that IFN-γ signaling does not influence viral persistence in the DRG. Two-tailed unpaired *t* test; n.s. n = 4–6 animals per group.

Figure S4. Neuronal stress markers and sciatic nerve structural alterations associated with persistent mechanical allodynia after CHIKV infection

(A) qPCR analysis of *Atf3* mRNA expression in dorsal root ganglia (DRG) from Mock, recovered (CHIKV-Recov.), and persistent (CHIKV-Persis.) mice. No significant differences were observed among groups. One-way ANOVA with Tukey's multiple-comparisons test, n.s. n = 5-6 animals per group.

(B) Total number of myelinated fibers in the sciatic nerve from Mock, CHIKV-Recov., and CHIKV-Persis. mice. Quantitative analysis revealed no differences in overall myelinated fiber density across groups. One-way ANOVA with Tukey's multiple-comparisons test, n.s. n = 4 animals per group.

(C) Representative images illustrating myelin abnormalities in the sciatic nerve of CHIKV-Persis. mice, including split myelin sheaths, myelin vacuolization, and redundant myelin, compared with Mock and CHIKV-Recov. groups.

(D, E) Neurofilament integrity in the sciatic nerve. **(D)** Representative immunofluorescence images of NF200 and **(E)** corresponding quantification show reduced neurofilament signal in CHIKV-Persis. mice compared with Mock and CHIKV-Recov. groups, consistent with axonal alterations associated with persistent mechanical allodynia. One-way ANOVA with Tukey's post hoc test; P = 0.041. n = 4 animals per group.

References

1. de Souza, W.M., and Weaver, S.C. (2024). Effects of climate change and human activities on vector-borne diseases. Nat Rev Microbiol *22*, 476–491. 10.1038/s41579-024-01026-0.
2. Ribeiro Dos Santos, G., Jawed, F., Mukandavire, C., Deol, A., Scarponi, D., Mboera, L.E.G., Seruyange, E., Poirier, M.J.P., Bosomprah, S., Udeze, A.O., et al. (2025). Global burden of chikungunya virus infections and the potential benefit of vaccination campaigns. Nat Med *31*, 2342–2349. 10.1038/s41591-025-03703-w.
3. de Souza, W.M., Lecuit, M., and Weaver, S.C. (2025). Chikungunya virus and other emerging arthritogenic alphaviruses. Nat Rev Microbiol *23*, 585–601. 10.1038/s41579-025-01177-8.
4. Naddaf, M. (2024). Mosquito-borne diseases are surging in Europe - how worried are scientists? Nature *633*, 749. 10.1038/d41586-024-03031-y.
5. Dupuis-Maguiraga, L., Noret, M., Brun, S., Le Grand, R., Gras, G., and Roques, P. (2012). Chikungunya disease: infection-associated markers from the acute to the chronic phase of arbovirus-induced arthralgia. PLoS Negl Trop Dis *6*, e1446. 10.1371/journal.pntd.0001446.
6. Doran, C., Duits, A., Tami, A., Gerstenbluth, I., and Bailey, A. (2023). "It's very saddening, you keep on wondering when the symptoms will be over": A qualitative study exploring the long-term chikungunya disease impact on daily life and well-being, 6 years after disease onset. PLoS Negl Trop Dis *17*, e0011793. 10.1371/journal.pntd.0011793.
7. Noor, F.M., Hossain, M.B., and Islam, Q.T. (2020). Prevalence of and risk factors for long-term disabilities following chikungunya virus disease: A meta-analysis. Travel Med Infect Dis *35*, 101618. 10.1016/j.tmaid.2020.101618.
8. Silva, M.M.O., Kikuti, M., Anjos, R.O., Portilho, M.M., Santos, V.C., Goncalves, T.S.F., Tauro, L.B., Moreira, P.S.S., Jacob-Nascimento, L.C., Santana, P.M., et al. (2021). Risk of chronic arthralgia and impact of pain on daily activities in a cohort of patients with chikungunya virus infection from Brazil. Int J Infect Dis *105*, 608–616. 10.1016/j.ijid.2021.03.003.
9. Mehta, R., Gerardin, P., de Brito, C.A.A., Soares, C.N., Ferreira, M.L.B., and Solomon, T. (2018). The neurological complications of chikungunya virus: A systematic review. Rev Med Virol *28*, e1978. 10.1002/rmv.1978.
10. Brito Ferreira, M.L., Militao de Albuquerque, M.F.P., de Brito, C.A.A., de Oliveira Franca, R.F., Porto Moreira, A.J., de Morais Machado, M.I., da Paz Melo, R., Medialdea-Carrera, R., Dornelas Mesquita, S., Lopes Santos, M., et al. (2020). Neurological disease in adults with Zika and chikungunya virus infection in Northeast Brazil: a prospective observational study. Lancet Neurol *19*, 826–839. 10.1016/S1474-4422(20)30232-5.
11. Supanchana, P., Kirushanth, C., Wijewardana, C.T., Peiris, L.T., Jayasinghe, J., Rudra, A., Govindapala, D., Higgoda, R., Thivakaran, T., Muthugala, R., et al. (2025). A case series of neuro-chikungunya: unmasking the neurotropic potential of chikungunya virus. BMC Infect Dis *26*, 32. 10.1186/s12879-025-12285-4.
12. Verma, R., Chakraborty, R., and Khetan, A. (2025). Chikungunya and Dengue Encephalitis: A Critical Narrative Review. Ann Indian Acad Neurol *28*, 314–322. 10.4103/aian.aian_28_25.
13. Porto Silva, C.N., Crispim, J.G., Pereira, M.C., Galdino da Rocha Pitta, M., Barreto de Melo Rego, M.J., and Melgarejo da Rosa, M. (2025). The communication between chikungunya infection and the central nervous system. Microb Pathog *206*, 107747. 10.1016/j.micpath.2025.107747.

14. de Souza, W.M., Fumagalli, M.J., de Lima, S.T.S., Parise, P.L., Carvalho, D.C.M., Hernandez, C., de Jesus, R., Delafiori, J., Candido, D.S., Carregari, V.C., et al. (2024). Pathophysiology of chikungunya virus infection associated with fatal outcomes. Cell Host Microbe *32*, 606–622 e608. 10.1016/j.chom.2024.02.011.
15. Maure, C., Khazhidinov, K., Kang, H., Auzenbergs, M., Moyersoen, P., Abbas, K., Santos, G.M.L., Medina, L.M.H., Wartel, T.A., Kim, J.H., et al. (2024). Chikungunya vaccine development, challenges, and pathway toward public health impact. Vaccine *42*, 126483. 10.1016/j.vaccine.2024.126483.
16. Mosnier, E., Jaffar-Bandjee, M.C., Cally, R., Dahmane, L., Frumence, E., Luong Nguyen, L.B., Manaquin, R., Vincent, M., Moiton, M.P., Gerardin, P., et al. (2025). Fatal Adverse Event After VLA1553 Chikungunya Vaccination in an Elderly Patient: A Case Report From Reunion Island. Open Forum Infect Dis *12*, ofaf550. 10.1093/ofid/ofaf550.
17. Gervais, A., Bastard, P., Zhang, Q., Jaffar-Bandjee, M.C., Bizien, L., Dahmane, L., Moiton, M.P., Jabot, J., Cally, R., Maillard, A., et al. (2026). Type I IFN autoantibodies underlie chikungunya live-attenuated vaccine encephalitis. Proc Natl Acad Sci U S A *123*, e2532212123. 10.1073/pnas.2532212123.
18. Tanabe, I.S.B., Santos, E.C., Tanabe, E.L.L., Souza, S.J.M., Santos, F.E.F., Taniele-Silva, J., Ferro, J.F.G., Lima, M.C., Moura, A.A., Anderson, L., and Bassi, E.J. (2019). Cytokines and chemokines triggered by Chikungunya virus infection in human patients during the very early acute phase. Trans R Soc Trop Med Hyg *113*, 730–733. 10.1093/trstmh/trz065.
19. Lozano-Parra, A., Herrera, V., Urcuqui-Inchima, S., Ramirez, R.M.G., and Villar, L.A. (2024). Acute Immunological Profile and Prognostic Biomarkers of Persistent Joint Pain in Chikungunya Fever: A Systematic Review. Yale J Biol Med *97*, 473–489. 10.59249/RQYJ3197.
20. Zarrella, K.M., Sheridan, R.M., Ware, B.C., Davenport, B.J., da Silva, M.O.L., Vyshenska, D., Martin, A.U., May, N.A., Weiskopf, D., Hesselberth, J.R., et al. (2025). Chikungunya virus persists in joint-associated macrophages and promotes chronic disease. Res Sq. 10.21203/rs.3.rs-6917990/v1.
21. Bezerra, W.P., Moizeis, R.N.C., Salmeron, A.C.A., Pereira, H.W.B., de Araujo, J.M.G., Guedes, P.M.M., Fernandes, J.V., and Nascimento, M.S.L. (2023). Innate immune response in patients with acute Chikungunya disease. Med Microbiol Immunol *212*, 279–290. 10.1007/s00430-023-00771-y.
22. Ninla-Aesong, P., Mitarnun, W., and Noipha, K. (2019). Proinflammatory Cytokines and Chemokines as Biomarkers of Persistent Arthralgia and Severe Disease After Chikungunya Virus Infection: A 5-Year Follow-Up Study in Southern Thailand. Viral Immunol *32*, 442–452. 10.1089/vim.2019.0064.
23. Brito, R.M.M., de Melo, M.F., Fernandes, J.V., Valverde, J.G., Matta Guedes, P.M., de Araujo, J.M.G., and Nascimento, M.S.L. (2024). Acute Chikungunya Virus Infection Triggers a Diverse Range of T Helper Lymphocyte Profiles. Viruses *16*. 10.3390/v16091387.
24. Casanova, J.L., MacMicking, J.D., and Nathan, C.F. (2024). Interferon-gamma and infectious diseases: Lessons and prospects. Science *384*, eadl2016. 10.1126/science.adl2016.
25. Tan, P.H., Ji, J., Yeh, C.C., and Ji, R.R. (2021). Interferons in Pain and Infections: Emerging Roles in Neuro-Immune and Neuro-Glial Interactions. Front Immunol *12*, 783725. 10.3389/fimmu.2021.783725.
26. Tsuda, M., Masuda, T., Kitano, J., Shimoyama, H., Tozaki-Saitoh, H., and Inoue, K. (2009). IFN-gamma receptor signaling mediates spinal microglia activation driving neuropathic pain. Proc Natl Acad Sci U S A *106*, 8032–8037. 10.1073/pnas.0810420106.

27. Benjamanukul, S., Osiri, M., Chansaenroj, J., Chirathaworn, C., and Poovorawan, Y. (2021). Rheumatic manifestations of Chikungunya virus infection: Prevalence, patterns, and enthesitis. PLoS One *16*, e0249867. 10.1371/journal.pone.0249867.
28. de Andrade, D.C., Jean, S., Clavelou, P., Dallel, R., and Bouhassira, D. (2010). Chronic pain associated with the Chikungunya Fever: long lasting burden of an acute illness. BMC Infect Dis *10*, 31. 10.1186/1471-2334-10-31.
29. Rueda-Lopes, F.C., Soares, C.N., Vieira, I.F., Mendonca, S., Martins, E.B., Lant, S., Sequeira, P.C., Solomon, T., de Filippis, A.M.B., Calvet, G., and Brasil, P. (2020). Bilateral median nerve neuritis after chikungunya virus infection. Lancet Infect Dis *20*, 382. 10.1016/S1473-3099(19)30741-8.
30. Silva, V.P., Costa, D.S., Carvalho, V., Garces, T., Barros, E.L.T., Oliveira, J.S., Pereira, A., and Ferreira, G.P. (2020). Peripheral polyneuropathy associated with Chikungunya virus infection. J Neurovirol *26*, 122–126. 10.1007/s13365-019-00782-7.
31. Sun, W., Shi, S., Liao, S., and Zhai, M. (2025). Chikungunya fever: pathogenesis and mechanisms underlying pain symptoms. Front Immunol *16*, 1679385. 10.3389/fimmu.2025.1679385.
32. Lories, R. (2011). The balance of tissue repair and remodeling in chronic arthritis. Nat Rev Rheumatol *7*, 700–707. 10.1038/nrrheum.2011.156.
33. Kamiya, N., Kuroyanagi, G., Aruwajoye, O., and Kim, H.K.W. (2019). IL6 receptor blockade preserves articular cartilage and increases bone volume following ischemic osteonecrosis in immature mice. Osteoarthritis Cartilage *27*, 326–335. 10.1016/j.joca.2018.10.010.
34. Chang, C.J., Chang, T.M., Sun, Y.S., Lin, J.F., Lee, C.W., Fang, M.L., and Liu, J.F. (2025). Lutein attenuates rheumatoid arthritis progression by suppressing MAPK/NF-kappaB signaling and MMP3 and MMP13 expression in fibroblast-like Synoviocytes. Int Immunopharmacol *164*, 115360. 10.1016/j.intimp.2025.115360.
35. Helwa-Shalom, O., Kahlon-Suki, Y., Markowitz, S.I., Goren, K., Shilo, D., Schoonmaker, S., Yochanan, C., Gellman, Y.N., Beyth, S., Deutsch, D., et al. (2025). Amelogenin Null Mice Develop Osteoarthritis, While Its Application Mitigates Disease Phenotypes in a Rat Model. FASEB J *39*, e70838. 10.1096/fj.202500827R.
36. Yuan, L., Li, Y., Liu, D., Zhang, H., Yang, J., Shen, H., Xia, L., Yao, L., and Lu, J. (2024). Interleukin-35 protein inhibits osteoclastogenesis and attenuates collagen-induced arthritis in mice. J Cell Physiol *239*, e31231. 10.1002/jcp.31231.
37. Finnerup, N.B., Kuner, R., and Jensen, T.S. (2021). Neuropathic Pain: From Mechanisms to Treatment. Physiol Rev *101*, 259–301. 10.1152/physrev.00045.2019.
38. Katz, H.R., Arcese, A.A., Bloom, O., and Morgan, J.R. (2022). Activating Transcription Factor 3 (ATF3) is a Highly Conserved Pro-regenerative Transcription Factor in the Vertebrate Nervous System. Front Cell Dev Biol *10*, 824036. 10.3389/fcell.2022.824036.
39. Pan, J.Z., Wang, Z., Sun, W., Pan, P., Li, W., Sun, Y., Chen, S., Lin, A., Tan, W., He, L., et al. (2024). ATF3 is a neuron-specific biomarker for spinal cord injury and ischaemic stroke. Clin Transl Med *14*, e1650. 10.1002/ctm2.1650.
40. Seijffers, R., Mills, C.D., and Woolf, C.J. (2007). ATF3 increases the intrinsic growth state of DRG neurons to enhance peripheral nerve regeneration. J Neurosci *27*, 7911–7920. 10.1523/JNEUROSCI.5313-06.2007.
41. Hunt, D., Raivich, G., and Anderson, P.N. (2012). Activating transcription factor 3 and the nervous system. Front Mol Neurosci *5*, 7. 10.3389/fnmol.2012.00007.
42. Dai, Y., Iwata, K., Fukuoka, T., Kondo, E., Tokunaga, A., Yamanaka, H., Tachibana, T., Liu, Y., and Noguchi, K. (2002). Phosphorylation of extracellular signal-regulated kinase in primary afferent neurons by noxious stimuli and its involvement in peripheral sensitization. J Neurosci *22*, 7737–7745. 10.1523/JNEUROSCI.22-17-07737.2002.

43. Gao, Y.J., and Ji, R.R. (2009). c-Fos and pERK, which is a better marker for neuronal activation and central sensitization after noxious stimulation and tissue injury? Open Pain J *2*, 11–17. 10.2174/1876386300902010011.
44. Goupil, B.A., and Mores, C.N. (2016). A Review of Chikungunya Virus-induced Arthralgia: Clinical Manifestations, Therapeutics, and Pathogenesis. Open Rheumatol J *10*, 129–140. 10.2174/1874312901610010129.
45. Mariz, C.A., de Oliveira, N.M.N., Alexandre, S.C.A., Viana, I., de Morais, C.N.L., Marques, E.T.A., Jaenisch, T., de Souza, W.V., Militao de Albuquerque, M.F.P., de Brito, C.A.A., and Braga, C. (2026). Symptomatic chikungunya and chronic post-infection arthralgia in a highly endemic setting in Northeastern Brazil, 2018-2019: Clinical characteristics, prevalence and associated factors. PLoS One *21*, e0328141. 10.1371/journal.pone.0328141.
46. Martins, E.B., Quintana, M.S.B., Silva, M.F.B., de Bruycker-Nogueira, F., Moraes, I.C.V., Rodrigues, C.D.S., Santos, C.C., Sampaio, S.A., Pina-Costa, A., Fabri, A.A., et al. (2023). Predictors of chronic joint pain after Chikungunya virus infection in the INOVACHIK prospective cohort study. J Clin Virol *169*, 105610. 10.1016/j.jcv.2023.105610.
47. Paixao, E.S., Rodrigues, L.C., Costa, M., Itaparica, M., Barreto, F., Gerardin, P., and Teixeira, M.G. (2018). Chikungunya chronic disease: a systematic review and meta-analysis. Trans R Soc Trop Med Hyg *112*, 301–316. 10.1093/trstmh/try063.
48. Jin, H.W., Ichikawa, H., Fujita, M., Yamaai, T., Mukae, K., Nomura, K., and Sugimoto, T. (2005). Involvement of caspase cascade in capsaicin-induced apoptosis of dorsal root ganglion neurons. Brain Res *1056*, 139–144. 10.1016/j.brainres.2005.07.025.
49. Sekiguchi, M., Sekiguchi, Y., Konno, S., Kobayashi, H., Homma, Y., and Kikuchi, S. (2009). Comparison of neuropathic pain and neuronal apoptosis following nerve root or spinal nerve compression. Eur Spine J *18*, 1978–1985. 10.1007/s00586-009-1064-z.
50. Zhang, H., Li, N., Li, Z., Li, Y., Yu, Y., and Zhang, L. (2022). The Involvement of Caspases in Neuroinflammation and Neuronal Apoptosis in Chronic Pain and Potential Therapeutic Targets. Front Pharmacol *13*, 898574. 10.3389/fphar.2022.898574.
51. Bae, J.Y., Kim, J.H., Cho, Y.S., Mah, W., and Bae, Y.C. (2015). Quantitative analysis of afferents expressing substance P, calcitonin gene-related peptide, isolectin B4, neurofilament 200, and Peripherin in the sensory root of the rat trigeminal ganglion. J Comp Neurol *523*, 126–138. 10.1002/cne.23672.
52. De Benedetti, F., Prencipe, G., Bracaglia, C., Marasco, E., and Grom, A.A. (2021). Targeting interferon-gamma in hyperinflammation: opportunities and challenges. Nat Rev Rheumatol *17*, 678–691. 10.1038/s41584-021-00694-z.
53. Reischer, G., Heinke, B., and Sandkuhler, J. (2020). Interferon-gamma facilitates the synaptic transmission between primary afferent C-fibres and lamina I neurons in the rat spinal dorsal horn via microglia activation. Mol Pain *16*, 1744806920917249. 10.1177/1744806920917249.
54. Ferrara, V., Toti, A., Ghelardini, C., and Di Cesare Mannelli, L. (2022). Interferon-gamma and neuropathy: balance between pain and neuroprotection. Neural Regen Res *17*, 2700–2701. 10.4103/1673-5374.339484.
55. Harre, U., and Schett, G. (2017). Cellular and molecular pathways of structural damage in rheumatoid arthritis. Semin Immunopathol *39*, 355–363. 10.1007/s00281-017-0634-0.
56. Pap, T., and Korb-Pap, A. (2015). Cartilage damage in osteoarthritis and rheumatoid arthritis--two unequal siblings. Nat Rev Rheumatol *11*, 606–615. 10.1038/nrrheum.2015.95.
57. Duan, X., Cai, L., Pham, C.T.N., Abu-Amer, Y., Pan, H., Brophy, R.H., Wickline, S.A., and Rai, M.F. (2021). Amelioration of Posttraumatic Osteoarthritis in Mice Using Intraarticular Silencing of Periostin via Nanoparticle-Based Small Interfering RNA. Arthritis Rheumatol *73*, 2249–2260. 10.1002/art.41794.

58. Yoshida, Y., Ogata, A., Kang, S., Ebina, K., Shi, K., Nojima, S., Kimura, T., Ito, D., Morimoto, K., Nishide, M., et al. (2015). Semaphorin 4D Contributes to Rheumatoid Arthritis by Inducing Inflammatory Cytokine Production: Pathogenic and Therapeutic Implications. Arthritis Rheumatol *67*, 1481–1490. 10.1002/art.39086.
59. Chen, W., Foo, S.S., Taylor, A., Lulla, A., Merits, A., Hueston, L., Forwood, M.R., Walsh, N.C., Sims, N.A., Herrero, L.J., and Mahalingam, S. (2015). Bindarit, an inhibitor of monocyte chemotactic protein synthesis, protects against bone loss induced by chikungunya virus infection. J Virol *89*, 581–593. 10.1128/JVI.02034-14.
60. Goupil, B.A., McNulty, M.A., Martin, M.J., McCracken, M.K., Christofferson, R.C., and Mores, C.N. (2016). Novel Lesions of Bones and Joints Associated with Chikungunya Virus Infection in Two Mouse Models of Disease: New Insights into Disease Pathogenesis. PLoS One *11*, e0155243. 10.1371/journal.pone.0155243.
61. Sengupta, S., and Tripathi, A. (2023). Evaluation of analgesic and prophylactic activity of curcumin against chikungunya-infected acute/chronic arthralgic mice. J Med Virol *95*, e28661. 10.1002/jmv.28661.
62. Choutka, J., Jansari, V., Hornig, M., and Iwasaki, A. (2022). Author Correction: Unexplained post-acute infection syndromes. Nat Med *28*, 1723. 10.1038/s41591-022-01952-7.
63. Dochnal, S.A., Cohen, S.P., Hutchinson, M.R., Miller, Y.I., and Yaksh, T.L. (2025). Virally-initiated pain states: phenotypes, mechanisms, and future directions. Front Pain Res (Lausanne) *6*, 1527106. 10.3389/fpain.2025.1527106.
64. Sipila, R., Kemp, H., Harno, H., Rice, A.S.C., and Kalso, E. (2021). Health-related quality of life and pain interference in two patient cohorts with neuropathic pain: breast cancer survivors and HIV patients. Scand J Pain *21*, 512–521. 10.1515/sjpain-2020-0177.
65. Guedon, J.M., Yee, M.B., Zhang, M., Harvey, S.A., Goins, W.F., and Kinchington, P.R. (2015). Neuronal changes induced by Varicella Zoster Virus in a rat model of postherpetic neuralgia. Virology *482*, 167–180. 10.1016/j.virol.2015.03.046.
66. Gilden, D., Mahalingam, R., Nagel, M.A., Pugazhenthi, S., and Cohrs, R.J. (2011). Review: The neurobiology of varicella zoster virus infection. Neuropathol Appl Neurobiol *37*, 441–463. 10.1111/j.1365-2990.2011.01167.x.
67. Liu, X., and Tang, S.J. (2023). Pathogenic mechanisms of human immunodeficiency virus (HIV)-associated pain. Mol Psychiatry *28*, 3613–3624. 10.1038/s41380-023-02294-7.
68. Acosta-Ampudia, Y., Monsalve, D.M., Castillo-Medina, L.F., Rodriguez, Y., Pacheco, Y., Halstead, S., Willison, H.J., Anaya, J.M., and Ramirez-Santana, C. (2018). Autoimmune Neurological Conditions Associated With Zika Virus Infection. Front Mol Neurosci *11*, 116. 10.3389/fnmol.2018.00116.
69. van den Pol, A.N., Zhang, X., Maher, S.E., and Bothwell, A.L.M. (2021). Immune cells enhance Zika virus-mediated neurologic dysfunction in brain of mice with humanized immune systems. Dev Neurobiol *81*, 389–399. 10.1002/dneu.22820.
70. Khoutorsky, A., and Price, T.J. (2018). Translational Control Mechanisms in Persistent Pain. Trends Neurosci *41*, 100–114. 10.1016/j.tins.2017.11.006.
71. Matusali, G., Colavita, F., Bordi, L., Lalle, E., Ippolito, G., Capobianchi, M.R., and Castilletti, C. (2019). Tropism of the Chikungunya Virus. Viruses *11*. 10.3390/v11020175.
72. Skidmore, A.M., and Bradfute, S.B. (2023). The life cycle of the alphaviruses: From an antiviral perspective. Antiviral Res *209*, 105476. 10.1016/j.antiviral.2022.105476.
73. Griffin, D.E., Levine, B., Ubol, S., and Hardwick, J.M. (1994). The effects of alphavirus infection on neurons. Ann Neurol *35 Suppl*, S23–27. 10.1002/ana.410350709.
74. Vernon, P.S., and Griffin, D.E. (2005). Characterization of an in vitro model of alphavirus infection of immature and mature neurons. J Virol *79*, 3438–3447. 10.1128/JVI.79.6.3438-3447.2005.

75. Wang, Y., Sun, Q., Hanani, M., Qu, J., Guo, X., Yang, W., Shao, T., Zheng, S., Qiao, S., Jia, Y., et al. (2025). Demyelination-related pain: role of lysophosphatidic acid in satellite glial cell-neuron crosstalk. J Transl Med *23*, 1425. 10.1186/s12967-025-07568-y.
76. Gillespie, C.S., Sherman, D.L., Fleetwood-Walker, S.M., Cottrell, D.F., Tait, S., Garry, E.M., Wallace, V.C., Ure, J., Griffiths, I.R., Smith, A., and Brophy, P.J. (2000). Peripheral demyelination and neuropathic pain behavior in periaxin-deficient mice. Neuron *26*, 523–531. 10.1016/s0896-6273(00)81184-8.
77. Dzreyan, V., Rodkin, S., Nikul, V., Pitinova, M., and Uzdensky, A. (2021). The Expression of E2F1, p53, and Caspase 3 in the Rat Dorsal Root Ganglia After Sciatic Nerve Transection. J Mol Neurosci *71*, 826–835. 10.1007/s12031-020-01705-6.
78. Dehkordi, M.H., Munn, R.G.K., and Fearnhead, H.O. (2022). Non-Canonical Roles of Apoptotic Caspases in the Nervous System. Front Cell Dev Biol *10*, 840023. 10.3389/fcell.2022.840023.
79. Xu, S., Li, H., Ai, Z., Guo, R., Cheng, H., and Wang, Y. (2024). Exploring viral neuropathic pain: Molecular mechanisms and therapeutic implications. PLoS Pathog *20*, e1012397. 10.1371/journal.ppat.1012397.
80. Cohen, S.P., Wang, E.J., Doshi, T.L., Vase, L., Cawcutt, K.A., and Tontisirin, N. (2022). Chronic pain and infection: mechanisms, causes, conditions, treatments, and controversies. BMJ Med *1*, e000108. 10.1136/bmjmed-2021-000108.
81. Adaes, S., Ferreira-Gomes, J., Mendonca, M., Almeida, L., Castro-Lopes, J.M., and Neto, F.L. (2015). Injury of primary afferent neurons may contribute to osteoarthritis induced pain: an experimental study using the collagenase model in rats. Osteoarthritis Cartilage *23*, 914–924. 10.1016/j.joca.2015.02.010.
82. Ferreira-Gomes, J., Adaes, S., Sousa, R.M., Mendonca, M., and Castro-Lopes, J.M. (2012). Dose-dependent expression of neuronal injury markers during experimental osteoarthritis induced by monoiodoacetate in the rat. Mol Pain *8*, 50. 10.1186/1744-8069-8-50.
83. Goncalves Dos Santos, G., Jimenez-Andrade, J.M., Woller, S.A., Munoz-Islas, E., Ramirez-Rosas, M.B., Ohashi, N., Ferreira Catroli, G., Fujita, Y., Yaksh, T.L., and Corr, M. (2020). The neuropathic phenotype of the K/BxN transgenic mouse with spontaneous arthritis: pain, nerve sprouting and joint remodeling. Sci Rep *10*, 15596. 10.1038/s41598-020-72441-5.
84. Leuchtweis, J., Segond von Banchet, G., Eitner, A., Ebbinghaus, M., and Schaible, H.G. (2020). Pain-related behaviors associated with persistence of mechanical hyperalgesia after antigen-induced arthritis in rats. Pain *161*, 1571–1583. 10.1097/j.pain.0000000000001852.
85. Miyamoto, S., Nakamura, J., Ohtori, S., Orita, S., Nakajima, T., Omae, T., Hagiwara, S., Takazawa, M., Suzuki, M., Suzuki, T., and Takahashi, K. (2017). Pain-related behavior and the characteristics of dorsal-root ganglia in a rat model of hip osteoarthritis induced by mono-iodoacetate. J Orthop Res *35*, 1424–1430. 10.1002/jor.23395.
86. Nascimento, D., Pozza, D.H., Castro-Lopes, J.M., and Neto, F.L. (2011). Neuronal injury marker ATF-3 is induced in primary afferent neurons of monoarthritic rats. Neurosignals *19*, 210–221. 10.1159/000330195.
87. Orita, S., Ishikawa, T., Miyagi, M., Ochiai, N., Inoue, G., Eguchi, Y., Kamoda, H., Arai, G., Toyone, T., Aoki, Y., et al. (2011). Pain-related sensory innervation in monoiodoacetate-induced osteoarthritis in rat knees that gradually develops neuronal injury in addition to inflammatory pain. BMC Musculoskelet Disord *12*, 134. 10.1186/1471-2474-12-134.
88. Su, J., Gao, T., Shi, T., Xiang, Q., Xu, X., Wiesenfeld-Hallin, Z., Hokfelt, T., and Svensson, C.I. (2015). Phenotypic changes in dorsal root ganglion and spinal cord in the collagen antibody-induced arthritis mouse model. J Comp Neurol *523*, 1505–1528. 10.1002/cne.23749.

89. Thakur, M., Rahman, W., Hobbs, C., Dickenson, A.H., and Bennett, D.L. (2012). Characterisation of a peripheral neuropathic component of the rat monoiodoacetate model of osteoarthritis. PLoS One *7*, e33730. 10.1371/journal.pone.0033730.
90. Dalton, D.K., Pitts-Meek, S., Keshav, S., Figari, I.S., Bradley, A., and Stewart, T.A. (1993). Multiple defects of immune cell function in mice with disrupted interferon-gamma genes. Science *259*, 1739–1742. 10.1126/science.8456300.
91. da Silva, M.O.L., Figueiredo, C.M., Neris, R.L.S., Guimaraes-Andrade, I.P., Gavino-Leopoldino, D., Miler-da-Silva, L.L., Valenca, H.D.M., Ladislau, L., de Lima, C.V.F., Coccarelli, F.M., et al. (2024). Chikungunya and Mayaro Viruses Induce Chronic Skeletal Muscle Atrophy Triggered by Pro-Inflammatory and Oxidative Response. Int J Mol Sci *25*. 10.3390/ijms25168909.
92. Maia, J., Machado, L.K.A., Fernandes, G.G., Vitorino, L.C., Antonio, L.S., Araujo, S.M.B., Colodeti, L.C., Fontes-Dantas, F.L., Zeidler, J.D., Saraiva, G.N., et al. (2024). Mitotherapy prevents peripheral neuropathy induced by oxaliplatin in mice. Neuropharmacology *245*, 109828. 10.1016/j.neuropharm.2023.109828.
93. Chaplan, S.R., Bach, F.W., Pogrel, J.W., Chung, J.M., and Yaksh, T.L. (1994). Quantitative assessment of tactile allodynia in the rat paw. J Neurosci Methods *53*, 55–63. 10.1016/0165-0270(94)90144-9.
94. Dias, F.C., Alves, V.S., Matias, D.O., Figueiredo, C.P., Miranda, A.L.P., Passos, G.F., and Costa, R. (2019). The selective TRPV4 channel antagonist HC-067047 attenuates mechanical allodynia in diabetic mice. Eur J Pharmacol *856*, 172408. 10.1016/j.ejphar.2019.172408.
95. Pinto, L.G., Talbot, J., Peres, R.S., Franca, R.F., Ferreira, S.H., Ryffel, B., Aves-Filho, J.C., Figueiredo, F., Cunha, T.M., and Cunha, F.Q. (2015). Joint production of IL-22 participates in the initial phase of antigen-induced arthritis through IL-1beta production. Arthritis Res Ther *17*, 235. 10.1186/s13075-015-0759-2.
96. Dudler, J., Renggli-Zulliger, N., Busso, N., Lotz, M., and So, A. (2000). Effect of interleukin 17 on proteoglycan degradation in murine knee joints. Ann Rheum Dis *59*, 529–532. 10.1136/ard.59.7.529.
97. Magnusson, M., Zare, F., and Tarkowski, A. (2006). Requirement of type I interferon signaling for arthritis triggered by double-stranded RNA. Arthritis Rheum *54*, 148–157. 10.1002/art.21517.
98. Alkhatib, O., da Costa, R., Gentry, C., Quallo, T., Bevan, S., and Andersson, D.A. (2019). Promiscuous G-Protein-Coupled Receptor Inhibition of Transient Receptor Potential Melastatin 3 Ion Channels by Gbetagamma Subunits. J Neurosci *39*, 7840–7852. 10.1523/JNEUROSCI.0882-19.2019.
99. Alvarado-Vazquez, P.A., Morado-Urbina, C.E., Castaneda-Corral, G., Acosta-Gonzalez, R.I., Kitaura, H., Kimura, K., Takano-Yamamoto, T., and Jimenez-Andrade, J.M. (2015). Intra-articular administration of an antibody against CSF-1 receptor reduces pain-related behaviors and inflammation in CFA-induced knee arthritis. Neurosci Lett *584*, 39–44. 10.1016/j.neulet.2014.09.053.
100. Raucci, F., Iqbal, A.J., Saviano, A., Minosi, P., Piccolo, M., Irace, C., Caso, F., Scarpa, R., Pieretti, S., Mascolo, N., and Maione, F. (2019). IL-17A neutralizing antibody regulates monosodium urate crystal-induced gouty inflammation. Pharmacol Res *147*, 104351. 10.1016/j.phrs.2019.104351.
101. Mendonca, H.R., Carvalho, J.N.A., Abreu, C.A., Mariano de Souza Aguiar Dos Santos, D., Carvalho, J.R., Marques, S.A., da Costa Calaza, K., and Martinez, A.M.B. (2018). Lack of Galectin-3 attenuates neuroinflammation and protects the retina and optic nerve of diabetic mice. Brain Res *1700*, 126–137. 10.1016/j.brainres.2018.07.018.

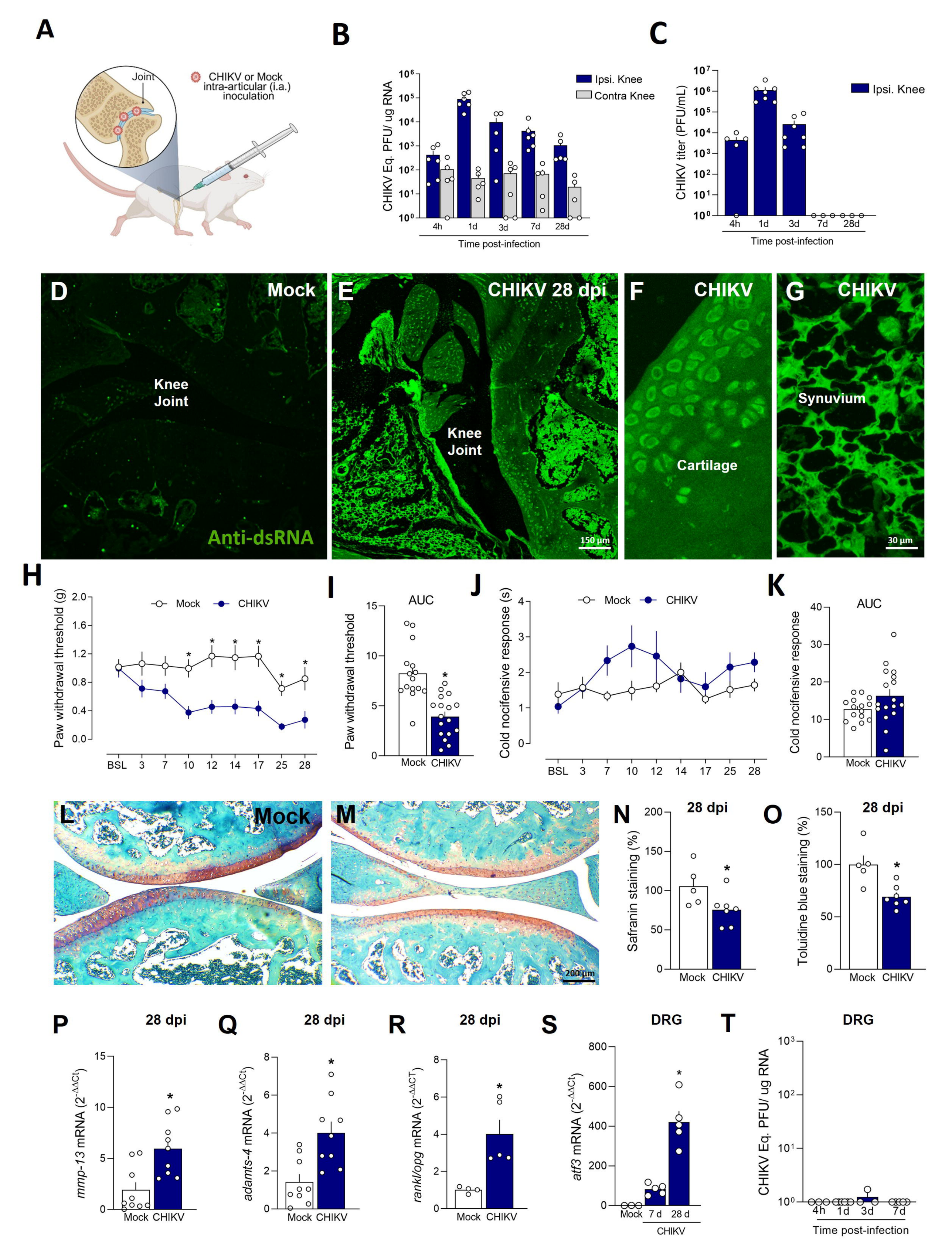
A
Joint
CHIKV or Mock intra-articular (i.a.) inoculation
B
Ipsi. Knee
Contra Knee
CHIKV Eq. PFU/ ug RNA
4h 1d 3d 7d 28d
Time post-infection
C
Ipsi. Knee
CHIKV titer (PFU/mL)
4h 1d 3d 7d 28d
Time post-infection
D Mock
Knee Joint
Anti-dsRNA
E CHIKV 28 dpi
Knee Joint
150 µm
F CHIKV
Cartilage
G CHIKV
Synuvium
30 µm
H
Mock CHIKV
Paw withdrawal threshold (g)
BSL 3 7 10 12 14 17 25 28
I
AUC
Paw withdrawal threshold
Mock CHIKV
J
Mock CHIKV
Cold nocifensive response (s)
BSL 3 7 10 12 14 17 25 28
K
AUC
Cold nocifensive response
Mock CHIKV
L Mock
M
200 µm
N 28 dpi
Safranin staining (%)
Mock CHIKV
O 28 dpi
Toluidine blue staining (%)
Mock CHIKV
P 28 dpi
mmp-13 mRNA (2^-ΔΔCt)
Mock CHIKV
Q 28 dpi
adamts-4 mRNA (2^-ΔΔCt)
Mock CHIKV
R 28 dpi
rankl/opg mRNA (2^-ΔΔCT)
Mock CHIKV
S DRG
atf3 mRNA (2^-ΔΔCt)
Mock 7 d 28 d
CHIKV
T DRG
CHIKV Eq. PFU/ ug RNA
4h 1d 3d 7d
Time post-infection

Figure 1

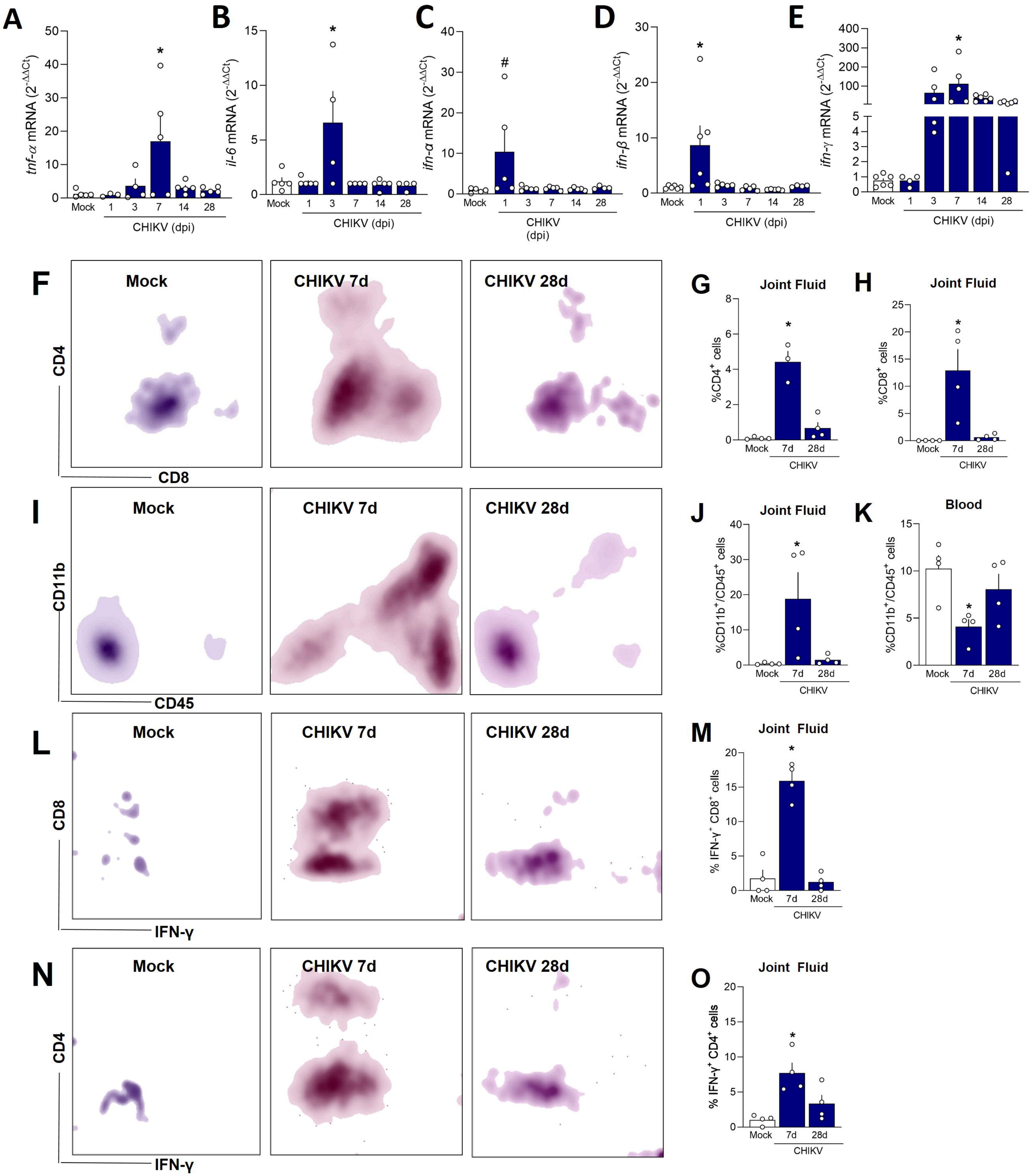
A
tnf-α mRNA (2^-ΔΔCt)
B
il-6 mRNA (2^-ΔΔCt)
C
ifn-α mRNA (2^-ΔΔCt)
D
ifn-β mRNA (2^-ΔΔCt)
E
ifn-γ mRNA (2^-ΔΔCt)
Mock
1
3
7
14
28
CHIKV (dpi)
F
Mock
CHIKV 7d
CHIKV 28d
CD4
CD8
G
Joint Fluid
%CD4+ cells
H
Joint Fluid
%CD8+ cells
I
CD11b
CD45
J
Joint Fluid
%CD11b+/CD45+ cells
K
Blood
L
IFN-γ
M
Joint Fluid
% IFN-γ+ CD8+ cells
N
O
Joint Fluid
% IFN-γ+ CD4+ cells
CHIKV

Figure 2

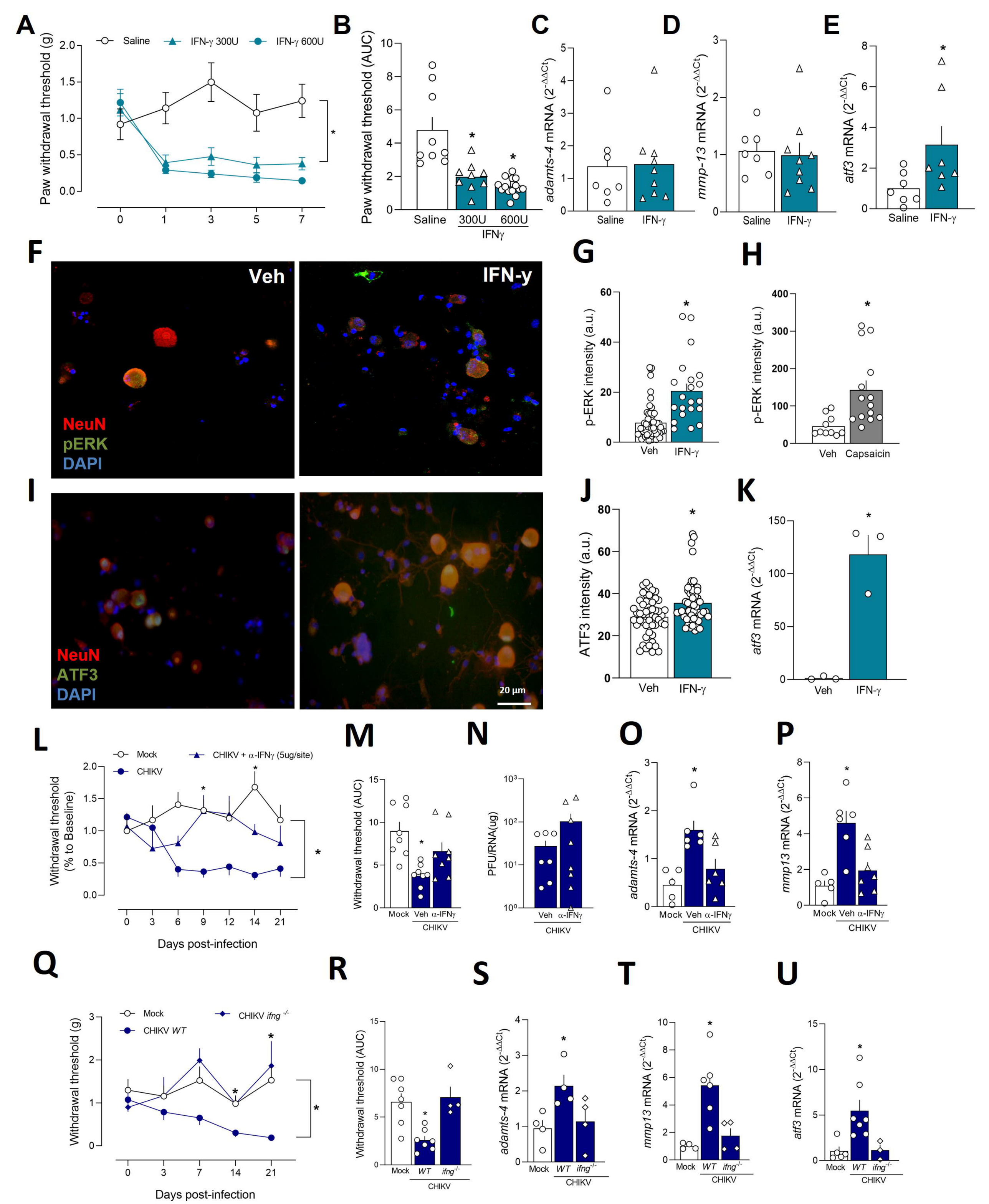
A
Saline
IFN-γ 300U
IFN-γ 600U
Paw withdrawal threshold (g)
Days post-infection
B
Paw withdrawal threshold (AUC)
Saline
300U
600U
IFNγ
C
adamts-4 mRNA (2^-ΔΔCt)
Saline
IFN-γ
D
mmp-13 mRNA (2^-ΔΔCt)
E
atf3 mRNA (2^-ΔΔCt)
F
Veh
IFN-y
NeuN
pERK
DAPI
G
p-ERK intensity (a.u.)
H
Capsaicin
I
ATF3
20 µm
J
ATF3 intensity (a.u.)
K
L
Mock
CHIKV
CHIKV + α-IFNγ (5ug/site)
Withdrawal threshold (% to Baseline)
M
Withdrawal threshold (AUC)
α-IFNγ
N
PFU/RNA(ug)
O
adamts-4 mRNA (2^-ΔΔCt)
P
mmp13 mRNA (2^-ΔΔCt)
Q
CHIKV ifng -/-
CHIKV WT
Withdrawal threshold (g)
R
S
T
U
ifng-/-
WT

Figure 3

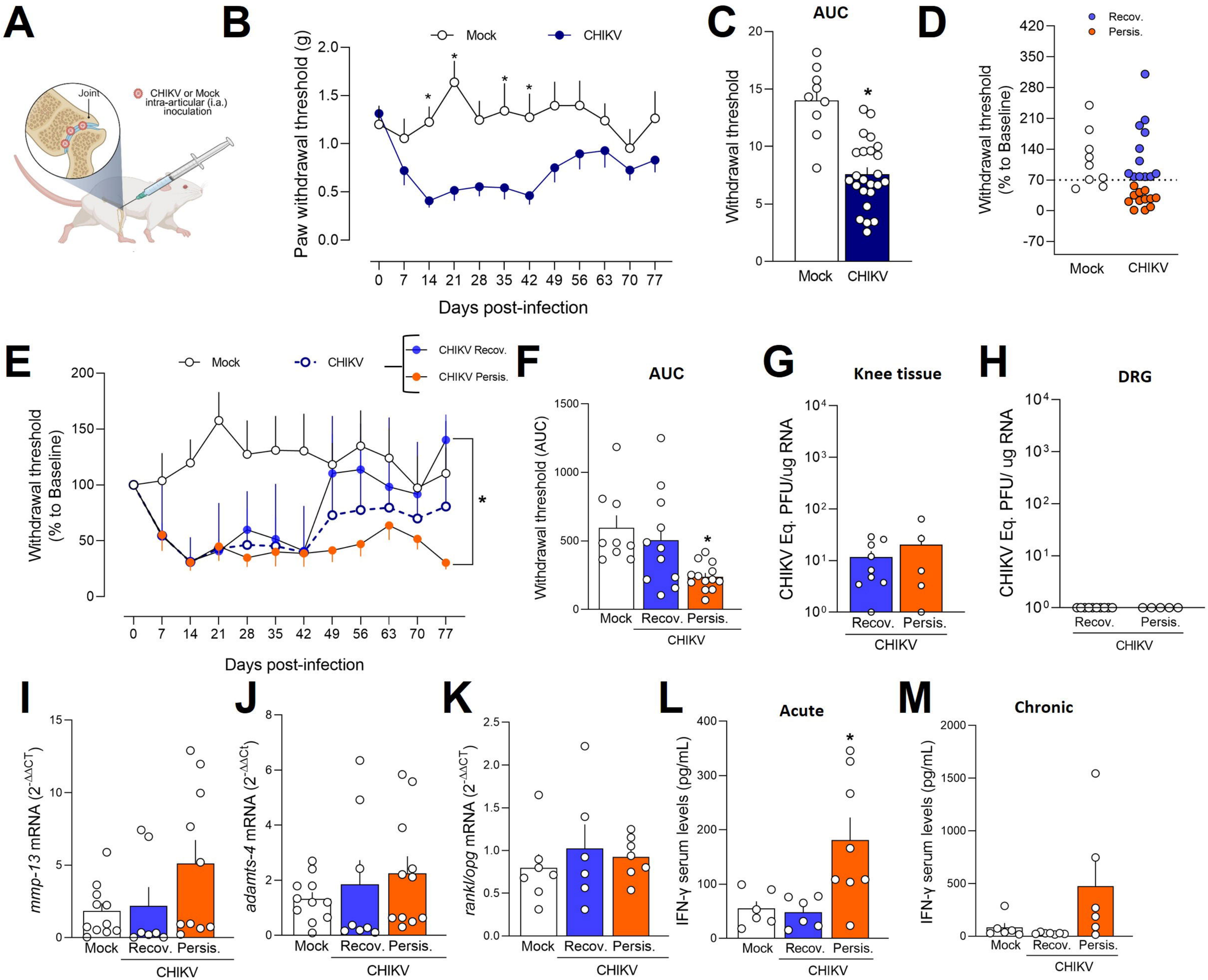
A
Joint
CHIKV or Mock intra-articular (i.a.) inoculation
B
Mock
CHIKV
Paw withdrawal threshold (g)
Days post-infection
C
AUC
Withdrawal threshold
Mock
CHIKV
D
Recov.
Persis.
Withdrawal threshold (% to Baseline)
Mock
CHIKV
E
Mock
CHIKV
CHIKV Recov.
CHIKV Persis.
Withdrawal threshold (% to Baseline)
Days post-infection
F
AUC
Withdrawal threshold (AUC)
Mock
Recov.
Persis.
CHIKV
G
Knee tissue
CHIKV Eq. PFU/ug RNA
Recov.
Persis.
CHIKV
H
DRG
CHIKV Eq. PFU/ ug RNA
Recov.
Persis.
CHIKV
I
mmp-13 mRNA (2^-ΔΔCT)
Mock
Recov.
Persis.
CHIKV
J
adamts-4 mRNA (2^-ΔΔCt)
Mock
Recov.
Persis.
CHIKV
K
rankl/opg mRNA (2^-ΔΔCT)
Mock
Recov.
Persis.
CHIKV
L
Acute
IFN-γ serum levels (pg/mL)
Mock
Recov.
Persis.
CHIKV
M
Chronic
IFN-γ serum levels (pg/mL)
Mock
Recov.
Persis.
CHIKV

Figure 4

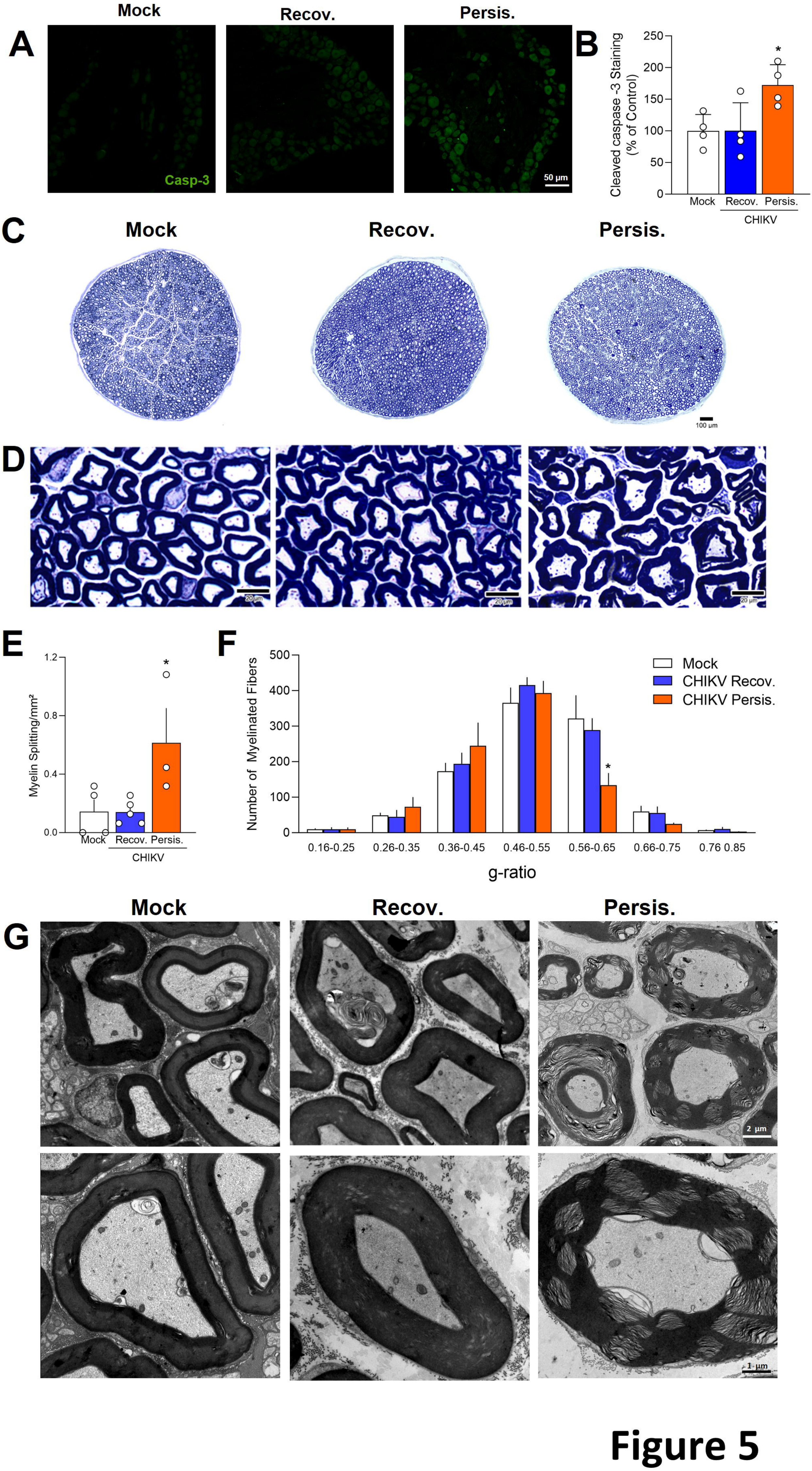
A
Mock
Recov.
Persis.
Casp-3
50 µm
B
Cleaved caspase -3 Staining (% of Control)
250
200
150
100
50
0
*
Mock
Recov.
Persis.
CHIKV
C
Mock
Recov.
Persis.
100 µm
D
20 µm
E
Myelin Splitting/mm²
1.2
0.8
0.4
0.0
*
Mock
Recov.
Persis.
CHIKV
F
Number of Myelinated Fibers
500
400
300
200
100
0
Mock
CHIKV Recov.
CHIKV Persis.
*
0.16-0.25
0.26-0.35
0.36-0.45
0.46-0.55
0.56-0.65
0.66-0.75
0.76 0.85
g-ratio
G
Mock
Recov.
Persis.
2 µm
1 µm

Figure 5

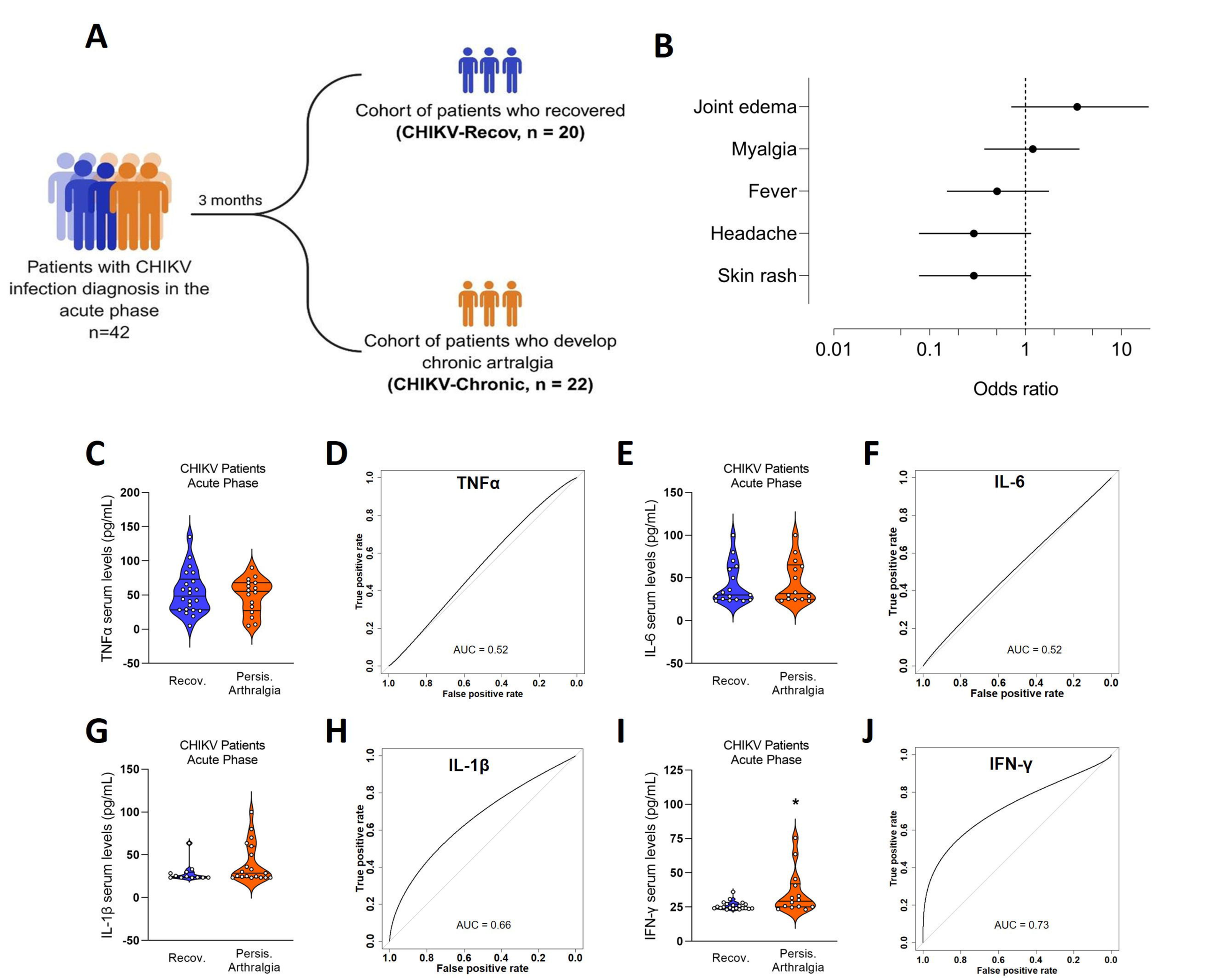
A
Patients with CHIKV infection diagnosis in the acute phase n=42
3 months
Cohort of patients who recovered (CHIKV-Recov, n = 20)
Cohort of patients who develop chronic artralgia (CHIKV-Chronic, n = 22)
B
Joint edema
Myalgia
Fever
Headache
Skin rash
0.01
0.1
1
10
Odds ratio
C
CHIKV Patients Acute Phase
TNFα serum levels (pg/mL)
Recov.
Persis. Arthralgia
D
TNFα
True positive rate
False positive rate
AUC = 0.52
E
CHIKV Patients Acute Phase
IL-6 serum levels (pg/mL)
Recov.
Persis. Arthralgia
F
IL-6
True positive rate
False positive rate
AUC = 0.52
G
CHIKV Patients Acute Phase
IL-1β serum levels (pg/mL)
Recov.
Persis. Arthralgia
H
IL-1β
True positive rate
False positive rate
AUC = 0.66
I
CHIKV Patients Acute Phase
IFN-γ serum levels (pg/mL)
*
Recov.
Persis. Arthralgia
J
IFN-γ
True positive rate
False positive rate
AUC = 0.73

Figure 6